# Lift-off of a single particle in Newtonian and viscoelastic fluids by direct numerical simulation

By N. A. PATANKAR†, P. Y. HUANG, T. KO
AND D. D. JOSEPH

Department of Aerospace Engineering and Mechanics and the Minnesota Supercomputer
Institute, University of Minnesota, Minneapolis, MN 55455, USA

In this paper we study the lift-off to equilibrium of a single circular particle in Newtonian and viscoelastic fluids by direct numerical simulation. A particle heavier than the fluid is driven forward on the bottom of a channel by a plane Poiseuille flow. After a certain critical Reynolds number, the particle rises from the wall to an equilibrium height at which the buoyant weight just balances the upward thrust from the hydrodynamic force. The aim of the calculation is the determination of the critical lift-off condition and the evolution of the height, velocity and angular velocity of the particle as a function of the pressure gradient and material and geometric parameters. The critical Reynolds number for lift-off is found to be larger for a heavier particle whereas it is lower for a particle in a viscoelastic fluid. A correlation for the critical shear Reynolds number for lift-off is obtained. The equilibrium height increases with the Reynolds number, the fluid elasticity and the slip angular velocity of the particle. Simulations of single particle lift-off at higher Reynolds numbers in a Newtonian fluid by Choi & Joseph (2001) but reported here show multiple steady states and hysteresis loops. This is shown here to be due to the presence of two turning points of the equilibrium solution.

## 1. Introduction

The theory of lift is one of the great achievements of aerodynamics. Airplanes take off, rise to a certain height and move forward under the balance of lift and weight. The lift and suspension of particles in the flow of slurries is another application in which lift plays a central role; in the oil industry we can consider the removal of drill cuttings in horizontal drill holes and sand transport in fractured reservoirs. The theory of lift for these particle applications is underdeveloped and in most simulators no lift forces are modelled. A force experienced by a particle moving through a fluid with circulation (or shearing motion for a viscous fluid) will be referred to as the lift force in this work.

Joseph (2001) proposed that problems of fluidization by lift can be decomposed into two separate types of study: (i) single particle studies in which the factors that govern lifting of a heavier-than-liquid particle off a wall by a shear flow are identified, and (ii) many particle studies in which cooperative effects on lift-off are important.

† Present address: Department of Mechanical Engineering, Northwestern University, Evanston, IL 60208, USA.

Different analytical expressions for the lift force on a single particle can be found in literature. They are based on perturbing Stokes flow with inertia or on perturbing potential flow with a little vorticity. The domain of parameters for which these analytical expressions are applicable is restricted. The perturbation analyses are valuable because they are analytical and explicit, but they are not directly applicable to engineering problems such as proppant transport, removal of drill cuttings, sediment transport or even lift-off of heavy single particles. Some formulae hold for particles in unbounded flows, others take the walls into account.

The aerodynamic lift on an airfoil with the ground effect is given by (see, e.g. Kuethe & Chow 1998) the potential flow theory. Circulation in the fluid gives rise to a lift force on a translating airfoil. A formula for the lift force on a sphere in an inviscid fluid, in which uniform motion is perturbed by weak shear, was derived by Auton (1987) and Drew & Passman (1999).

The experiments of Segré & Silberberg (1961, 1962) have had a great influence on studies of the fluid mechanics of migration and lift at low Reynolds number. Rubinow & Keller (1961) derived a formula for the transverse force on a sphere rotating and translating in a viscous fluid which is at rest at infinity. The theory of Rubinow & Keller (1961) is valid for a sphere in uniform flow but Couette and poiseuille flows are not uniform. Bretherton (1962) derived an expression for the lift force on a cylinder in an unbounded linear shear flow. Saffman (1965) gave a similar expression for the lift on a sphere in an unbounded linear shear flow. He concluded that the lift force due to particle rotation is less by an order of magnitude than that due to shear when the Reynolds number is small. Asmolov (1990) and, independently, McLaughlin (1991) generalized Saffman's analysis to remove certain restrictions on the flow parameters.

Dandy & Dwyer (1990) and Cherukat, McLaughlin & Dandy (1999) reported computational studies of the inertial lift on a sphere in linear shear flows. Mei (1992) obtained an expression for the lift force by fitting an equation to Dandy & Dwyer's (1990) data for high Reynolds numbers and Saffman's expression for low Reynolds numbers. The numerical results of Dandy & Dwyer (1990) are said to be valid for non-rotating spheres. Hence they cannot be applied, strictly speaking, to the case of freely rotating spheres in shear flows. Kurose & Komori (1999) performed numerical simulations to determine the drag and lift forces on rotating spheres in an unbounded linear shear flow.

The problem of inertial lift on a moving sphere in contact with a plane wall in shear flow has been analysed as a perturbation of Stokes flow with inertia by Leighton & Acrivos (1985), Cherukat & McLaughlin (1994) and Krishnan & Leighton (1995). These studies lead to specific and useful analytical results expressed in terms of the translational and rotational velocities of the sphere and the shear rate. The lift on a stationary sphere off a wall in a shear flow varies as the fourth power of the radius and the square of the shear rate. If the shear Reynolds number is sufficiently large, the lift force exceeds the gravitational force and the sphere separates from the wall.

Hogg (1994) studied the inertial migration of non-neutrally buoyant spherical particles in two-dimensional shear flows. The inertial lift on a spherical particle in plane Poiseuille flow at large-channel Reynolds numbers was studied by Asmolov (1999). The effect of curvature of the unperturbed velocity profile was found to be important. Details of the theoretical analysis of lift are also given by Brenner (1966), Cox & Mason (1971), Leal (1980) and Feuillebois (1989), among others.

Eichhorn & Small (1964) performed experiments to study the lift and drag forces

on spheres suspended in a Poiseuille flow. Bagnold (1974) studied the fluid forces on a body in shear flow experimentally. Ye & Roco (1991) measured the angular velocity of neutrally buoyant particles in a planar Couette flow experimentally. Liu *et al.* (1993), Liu & Joseph (1993) and Joseph *et al.* (1994) studied experimentally the effect of a wall on particles sedimenting in a viscoelastic fluid. Singh & Joseph (2000) performed numerical simulation of the sedimentation of a sphere near a wall in viscoelastic fluids.

Analytical investigation of the lift on a sphere moving very close to an infinite plane wall in a shear flow of a second-order fluid was carried out by Hu & Joseph (1999). The sphere was allowed to rotate and translate. They found that, owing to the normal stress effect, the flow gives rise to a positive elastic lift force on the sphere when the gap between the sphere and the wall is small. They concluded that smaller particles would be easier to suspend owing to the elastic lift in contrast to the inertial lift, which does not suspend small particles.

Direct two-dimensional simulations of the motion of circular particles in wall-bounded Couette and Poiseuille flows of a Newtonian fluid were made by Feng, Hu & Joseph (1994). Feng, Huang & Joseph (1995) studied numerically the lift force on an elliptic particle in pressure driven flows of Newtonian fluids. Numerical investigation of the motion of circular particles in Couette and Poiseuille flows of an Oldroyd-B fluid was carried out by Huang *et al.* (1997). We use the same numerical method, described in detail by Hu (1996), Hu & Patankar (2001) and Hu, Patankar & Zhu (2001), to study the lift-off of a single particle in Newtonian and viscoelastic fluids. It is an arbitrary Lagrangian–Eulerian (ALE) numerical method using body-fitted unstructured finite-element grids to simulate particulate flows. A closely related numerical method for particulate flows, based on a Chorin (1968) type fractional step scheme, was introduced by Choi (2000). Choi & Joseph (2001) use this scheme to study the fluidization by lift of 300 circular particles in a plane Poiseuille flow by direct numerical simulation.

In this paper, we examine the proposition that a freely translating neutrally buoyant sphere (or circle) in an unbounded linear shear flow moves with the fluid and experiences no lift independent of its angular velocity. Two-dimensional numerical simulations are performed in which a particle heavier than the fluid is lifted from the bottom of a horizontal channel by pressure driven (plane Poiseuille) flow. The buoyant weight of the particle is balanced by a force transverse to the axial direction of the channel. Similar simulations of particles lifted from the bottom of a horizontal channel by simple shear (Couette) flow are reported in Zhu (2000). We discuss the turning-point bifurcation phenomenon, first observed by Choi & Joseph (2001), in the lift-off of a single particle in Poiseuille flows. We propose a general data structure for the interrogation of numerical simulations to be used in developing a theory of fluidization by lift.

The governing equations, various parameters of the problem and a brief discussion on the lift models for solid–liquid flows will be presented in §2. Discussion of the lift force on a particle in an unbounded linear shear flow will be presented in §3. Results for lift-off of a single particle in Poiseuille flows in Newtonian fluids will be presented in §4. In §5 we will discuss the relative contributions to the lift force from pressure and shear. Results on the turning-point bifurcation phenomenon will be given in §6. Lift-off results in Oldroyd-B fluids will be presented in §7 and conclusions in §8.

## 2. Governing equations and the parameters of the problem

The governing equations for the fluid are

$$
\left.
\begin{aligned}
&\nabla \cdot \boldsymbol{u} = 0, \\
&\rho_f \left( \frac{\partial \boldsymbol{u}}{\partial t} + (\boldsymbol{u} \cdot \nabla)\boldsymbol{u} \right) = -\nabla P + \rho_f \boldsymbol{g} + \nabla \cdot \boldsymbol{T}, \\
&\boldsymbol{T} = \eta \boldsymbol{A} \quad \text{for a Newtonian fluid,} \\
&\boldsymbol{T} + \lambda_1 \overset{\triangledown}{\boldsymbol{T}} = \eta \left( \boldsymbol{A} + \lambda_2 \overset{\triangledown}{\boldsymbol{A}} \right) \quad \text{for an Oldroyd-B fluid,}
\end{aligned}
\right\}
\tag{1}
$$

where $\boldsymbol{u}(\boldsymbol{x},t)$ is the fluid velocity, $\rho_f$ is the fluid density, $P(\boldsymbol{x},t)$ is the pressure, $\boldsymbol{T}$ is the extra-stress tensor, $\boldsymbol{g}$ is the acceleration due to gravity, $\eta$ is the viscosity of the fluid, $\boldsymbol{A} = (\nabla \boldsymbol{u} + \nabla \boldsymbol{u}^T)$ is twice the deformation-rate tensor, $\lambda_1$ and $\lambda_2$ are the constant relaxation and retardation times, respectively; the Oldroyd-B model reduces to a Newtonian fluid when $\lambda_1 = \lambda_2$. $\overset{\triangledown}{\boldsymbol{T}}$ and $\overset{\triangledown}{\boldsymbol{A}}$ are the upper-convected derivatives of $\boldsymbol{T}$ and $\boldsymbol{A}$, respectively.

The equations of motion of the solid particles in a general three-dimensional case are

$$
\left.
\begin{aligned}
&m\frac{\mathrm{d}\boldsymbol{U}_p}{\mathrm{d}t} = m\boldsymbol{g} + \oint [-P\boldsymbol{1} + \boldsymbol{T}] \cdot \boldsymbol{n}\,\mathrm{d}\Gamma, \\
&\frac{\mathrm{d}(\boldsymbol{I} \cdot \boldsymbol{\Omega}_p)}{\mathrm{d}t} = \oint (\boldsymbol{x} - \boldsymbol{X}) \times ([-P\boldsymbol{1} + \boldsymbol{T}] \cdot \boldsymbol{n})\,\mathrm{d}\Gamma,
\end{aligned}
\right\}
\tag{2}
$$

where $m$ is the mass of the particle, $\boldsymbol{U}_p$ is the translational velocity, $\boldsymbol{\Omega}_p$ is the angular velocity, $\boldsymbol{I}$ is the moment-of-inertia tensor, $\boldsymbol{X}$ is the coordinate of the centre of mass of the particle and $\boldsymbol{1}$ is the unit tensor. Equations for the particle positions are obtained from the definition of velocity. The no-slip condition is imposed on the particle boundaries:

$$
\boldsymbol{u} = \boldsymbol{U}_p + \boldsymbol{\Omega}_p \times (\boldsymbol{x} - \boldsymbol{X}).
\tag{3}
$$

All the computations presented in this paper are carried out using dimensional parameters. Direct numerical simulation (DNS) of the motion of particles in fluids is carried out using a two-dimensional generalized Galerkin finite-element method which incorporates both the fluid and particle equations of motion into a single coupled variational equation. An arbitrary Lagrangian–Eulerian (ALE) moving mesh technique is used to account for the changes in the fluid domain owing to the motion of the particles. The EVSS (elastic-viscous-stress-split) scheme is used to simulate the motion of the particles in Oldroyd-B fluids. We use a triangular finite-element mesh. The mesh nodes on the particle surface move with the particle. Mesh velocities at the interior nodes are calculated by solving a Laplace equation. At each timestep, the particle positions and the mesh nodes are updated explicitly, while the velocities of the fluid and the solid particles are determined implicitly. If unacceptable element distortion is detected in the updated mesh, a new finite-element mesh is generated and the flow fields are projected from the old mesh to the new mesh. More details of our numerical scheme are given by Hu (1996), Hu & Patankar (2001) and Hu *et al.* (2001).

The computational domain for our simulations is shown in figure 1. We performed simulations in a periodic domain or in a computational domain which moves in the *x*-direction and is such that the particle is always at its centre. The inflow and
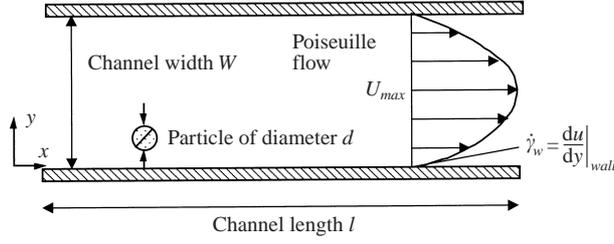
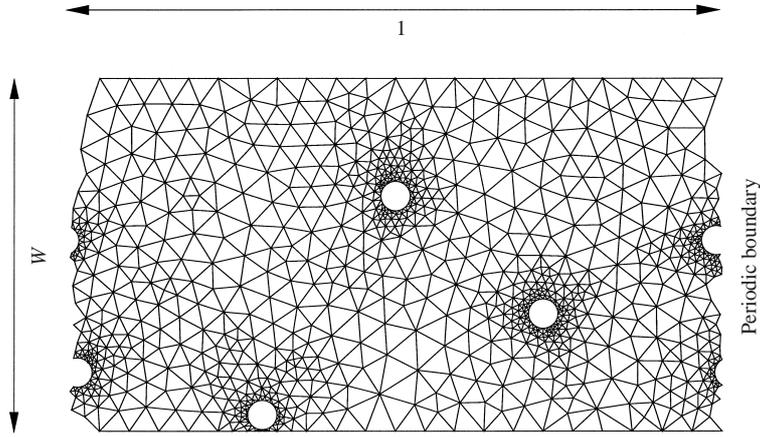FIGURE 1. Computational domain for the lift-off of a single particle in plane Poiseuille flow.



FIGURE 2. Unstructured mesh in a periodic domain.

outflow boundaries are located at a specified distance from the centre of the particle. A fully developed parabolic velocity profile, $u(y) = (\bar{p}/2\eta)(W - y)y$, corresponding to the applied pressure gradient is imposed at the inflow and outflow boundaries. The applied pressure gradient is given by $-\bar{p}$ and can be represented in terms of pressure at the inlet and the outlet of the channel; the pressure at the inlet is higher than that at the outlet.

In simulations in periodic domains (see figure 2) we split the pressure as follows:

$$P = p + \rho_f \boldsymbol{g} \cdot \boldsymbol{x} - \bar{p}\boldsymbol{e}_x \cdot \boldsymbol{x}$$

$$\Rightarrow -\nabla P = -\nabla p - \rho_f \boldsymbol{g} + \bar{p}\boldsymbol{e}_x \tag{4}$$

Where $\boldsymbol{e}_x$ is the unit vector in the $x$-direction and $\boldsymbol{x}$ is the position vector of any point in the domain. We solve for $p$ in our simulations. The external pressure gradient term then appears as a body-force-like term in the fluid and particle equations. The two methods of calculation, moving and periodic domains, give rise to nearly the same solution.

The set-up for our initial-value computation is described below. The particle is initially placed close to the bottom wall of the channel. Gravity acts in the negative $y$-direction. At $t = 0_+$, the fluid in the channel is driven by a pressure gradient along the $x$-direction. If the applied pressure gradient is large enough, the particle levitates. For the parameters we have considered, the particle rises to an equilibrium height (figure 3) above the bottom wall. In this state of steady motion the particle has an identically zero acceleration. The particle translational ($x$-direction) and angular velocities are constant. Since the particle is allowed to move freely, the net drag (force
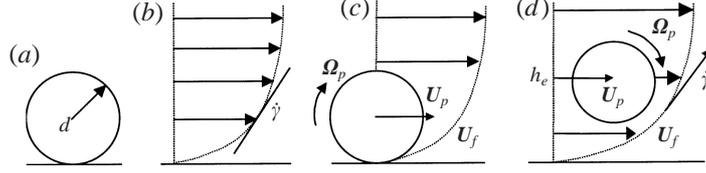
FIGURE 3. Lift-off and levitation to equilibrium.

in the $x$-direction) and torque on the particle is zero at steady state. The hydrodynamic lift force (acting along the $y$-direction) balances the net buoyant weight of the particle. At steady state, equation (2) becomes

$$(\rho_p - \rho_f)V_p\boldsymbol{g} + \bar{p}V_p\boldsymbol{e}_x + \oint [-p\mathbf{1} + \boldsymbol{T}] \cdot \boldsymbol{n}\,\mathrm{d}\Gamma = 0,$$

$$\oint (\boldsymbol{x} - \boldsymbol{X}) \times ([-p\mathbf{1} + \boldsymbol{T}] \cdot \boldsymbol{n})\,\mathrm{d}\Gamma = 0, \tag{5}$$

where $V_p$ is the volume per unit length of the circular particle and $\rho_p$ is the density of the particle. The slip velocity $U_f - U_p$ and the angular slip velocity $\Omega_f - \Omega_p = \frac{1}{2}\dot{\gamma} - \Omega_p$ are positive (figure 3).

A dimensionless description of the governing equations can be constructed by introducing scales: the particle size $d$ for length, $V$ for velocity, $d/V$ for time, $\eta V/d$ for stress and pressure, and $V/d$ for angular velocity of the particle. We choose $V = \dot{\gamma}_w d$, where $\dot{\gamma}_w$ is the shear rate at the wall (in the absence of the particle) as shown in figure 1. The wall shear rate is given by

$$\dot{\gamma}_w = \frac{W}{2\eta}\bar{p}. \tag{6}$$

The non-dimensional equations for a general three-dimensional case are (we use the same symbols for non-dimensional variables):

$$\nabla \cdot \boldsymbol{u} = 0,$$

$$R\left(\frac{\partial \boldsymbol{u}}{\partial t} + (\boldsymbol{u} \cdot \nabla)\boldsymbol{u}\right) = -\nabla p + 2\frac{d}{W}\boldsymbol{e}_x + \nabla \cdot \boldsymbol{T},$$

$$\boldsymbol{T} = \boldsymbol{A} \quad \text{for a Newtonian fluid,}$$

$$\boldsymbol{T} + \mathrm{De}\,\overset{\triangledown}{\boldsymbol{T}} = \left(\boldsymbol{A} + \frac{\lambda_2}{\lambda_1}\mathrm{De}\overset{\triangledown}{\boldsymbol{A}}\right) \quad \text{for an Oldroyd-B fluid,} \tag{7a}$$

$$\frac{\rho_p}{\rho_f}R\frac{m}{\rho_p d^3}\frac{\mathrm{d}U_p}{\mathrm{d}t} = -G\frac{m}{\rho_p d^3}\boldsymbol{e}_y + 2\frac{d}{W}\frac{m}{\rho_p d^3}\boldsymbol{e}_x + \oint [-p\mathbf{1} + \boldsymbol{T}] \cdot \boldsymbol{n}\,\mathrm{d}\Gamma,$$

$$\frac{\rho_p}{\rho_f}R\frac{\mathrm{d}([\boldsymbol{I}/\rho_p d^5] \cdot \boldsymbol{\Omega}_p)}{\mathrm{d}t} = \oint (\boldsymbol{x} - \boldsymbol{X}) \times ([-p\mathbf{1} + \boldsymbol{T}] \cdot \boldsymbol{n})\,\mathrm{d}\Gamma,$$

where $\boldsymbol{e}_y$ is the unit vector in the $y$-direction. We have used $\boldsymbol{g} = -g\boldsymbol{e}_y$. Equation (7a) and the corresponding initial and boundary conditions define an initial boundary-value problem that can be solved by direct numerical simulation. Particle positions are updated explicitly based on the values of velocity. The particle equations of motion

for a two-dimensional case become

$$\left.\begin{array}{l}
\dfrac{\rho_p}{\rho_f}R\dfrac{\mathrm{d}\boldsymbol{U}_p}{\mathrm{d}t} = -Ge_y + 2\dfrac{d}{W}e_x + \dfrac{4}{\pi}\oint [-p\boldsymbol{1} + \boldsymbol{T}]\cdot\boldsymbol{n}\,\mathrm{d}\Gamma, \\[4mm]
\dfrac{\rho_p}{\rho_f}R\dfrac{\mathrm{d}\boldsymbol{\Omega}_p}{\mathrm{d}t} = \dfrac{32}{\pi}\oint (\boldsymbol{x} - \boldsymbol{X})\times([-p\boldsymbol{1} + \boldsymbol{T}]\cdot\boldsymbol{n})\,\mathrm{d}\Gamma,
\end{array}\right\} \tag{7b}$$

where we consider circular particles of diameter $d$ with the mass per unit length $m = \frac{1}{4}\rho_p\pi d^2$ and the moment of inertia per unit length $I = \frac{1}{32}\rho_p\pi d^4$. The fluid equations of motion are the same as given in (7a). The parameters in this problem with the above choice of scaling are:

$$R = \frac{\rho_f V d}{\eta} = \frac{\rho_f\dot{\gamma}_w d^2}{\eta} = \frac{\rho_f W d^2}{2\eta^2}\bar{p} \qquad \text{shear Reynolds number,}$$

$$G = \frac{(\rho_p - \rho_f)gd^2}{\eta V},$$

$$= \frac{(\rho_p - \rho_f)gd}{\eta\dot{\gamma}_w} = \left(\frac{d}{w}\right)\frac{2(\rho_p - \rho_f)g}{\bar{p}} \qquad \text{gravity parameter,}$$

$$\rho_p/\rho_f \qquad \text{density ratio,}$$

$$\bar{p}d^2/\eta V = \bar{p}d/\eta\dot{\gamma}_w = 2d/W \qquad \text{aspect ratio,}$$

$$\mathrm{De} = \lambda_1 V/d = \lambda_1\dot{\gamma}_w = \lambda_1(W/2\eta)\bar{p} \qquad \text{Deborah number,}$$

$$\lambda_2/\lambda_1 \qquad \text{ratio of retardation and relaxation times.}$$

The velocity scale $V_g$ of a particle sedimenting in a viscous fluid is given by

$$V_g = \frac{(\rho_p - \rho_f)gd^2}{\eta}. \tag{8}$$

The gravity parameter $G$ represents the ratio of $V_g$ and $V$. For given material properties and the particle size, $RG = R_G = \rho_f(\rho_p - \rho_f)gd^3/\eta^2$ is constant and represents the Reynolds number based on the sedimentation velocity scale $V_g$. The value of the gravity Reynolds number $R_G$ is larger when the particle is heavier. The ratio $R/G = d\dot{\gamma}_w^2/((\rho_p/\rho_f - 1)g)$, which measures the ratio of inertia to buoyant weight, is a generalized Froude number.

The channel length $l$ is chosen large enough so that the solution is only weakly dependent on its value. The equilibrium height, $h_e$, of the particle depends on the parameters listed above:

$$\frac{h_e}{d} = f\left(R, G, \frac{d}{W}, \mathrm{De}, \frac{\lambda_2}{\lambda_1}\right). \tag{9}$$

Note that $\rho_p/\rho_f$ does not appear as a parameter in (9). It appears as the coefficient of acceleration terms in the particle equations (equations (7a) and (7b)). Since the acceleration of the particle in steady state is zero (equation (5)), $\rho_p/\rho_f$ is not a parameter in (9). For a Newtonian suspending fluid the last two parameters are not present.

The lift force on a circular particle in a Poiseuille flow of an Oldroyd-B fluid depends on various parameters,

$$L = f_1(\bar{p}, h_e, \Omega_p, U_p, \rho_f, \eta, \lambda_1, \lambda_2, d, W). \tag{10}$$

On non-dimensionalizing (Buckingham's Pi theorem) we obtain

$$\frac{L\rho_f d}{\eta^2} = f_2\left(R, \frac{d}{W}, \frac{h_e}{d}, \frac{\rho_f \Omega_p d^2}{\eta}, \frac{\rho_f U_p d}{\eta}, De, \frac{\lambda_2}{\lambda_1}\right), \tag{11}$$

where $L = (\frac{1}{4}\pi d^2)(\rho_p - \rho_f)g$ (the effective weight) at equilibrium if gravity acts along the transverse direction. A general expression for the lift force should depend on the parameters listed in (11). We may also replace $R$ and $d/W$ in (11) with a Reynolds number based on the fluid shear rate and the non-dimensional curvature, both at the location of the particle centre (in the absence of the particle). Equation (9) is implied by the more general equation (11) for a freely moving particle in a horizontal channel.

Modelling of solid–liquid mixtures has been approached in two ways. The first approach is to consider the solid–liquid mixture as an effective fluid medium. Bulk properties (such as the effective viscosity) of the composite mixture are then modelled. In the second approach, the solid and the fluid are considered as interpenetrating mixtures which are governed by the conservation laws. Interactions between the interpenetrating phases are modelled in the mixture theory approach. Models for the drag and lift forces on particles in solid–liquid mixtures are a complicated issue. The theory of fluidizing beds and sedimenting suspensions in which drag is important usually rely on the well-known Richardson–Zaki correlation (Richardson & Zaki 1954). Models for lift forces in mixtures are much less well developed than models for drag, but these models may also take form as a composition of the lift on a single particle and as a yet unknown function of the volume fraction.

## 3. Lift on a particle in an unbounded linear shear flow

Bretherton's (1962) expression for the lift and drag force (per unit length) $L$, on a cylinder in an unbounded linear shear flow is given by

$$\left.\begin{aligned}
L &= \frac{21.16\eta U_s}{\left(0.679 - \ln\left(\sqrt{\frac{1}{4}R}\right)\right)^2 + 0.634}, \\[2mm]
D &= \frac{4\pi\eta U_s\left(0.91 - \ln\left(\sqrt{\frac{1}{4}R}\right)\right)}{\left(0.679 - \ln\left(\sqrt{\frac{1}{4}R}\right)\right)^2 + 0.634}, \\[2mm]
R &= \frac{\rho_f \dot{\gamma} d^2}{\eta},
\end{aligned}\right\} \tag{12}$$

where $\dot{\gamma}$ is the shear rate. Saffman (1965) gave an expression for the lift force on a sphere in an unbounded linear shear flow

$$L = 6.46\frac{\eta d U_s}{4}\sqrt{R}, \tag{13}$$

Both the expressions are valid for small values of $R$. In (12) and (13), $U_s$ is the magnitude of velocity of the particle relative to the fluid. The direction of the lift force is such that it acts to deflect the particle towards the streamlines moving in the direction opposite to $U_s$. The balance between the net buoyant weight of a particle and the hydrodynamic lift force (equations (12) or (13)) leads to an expression for
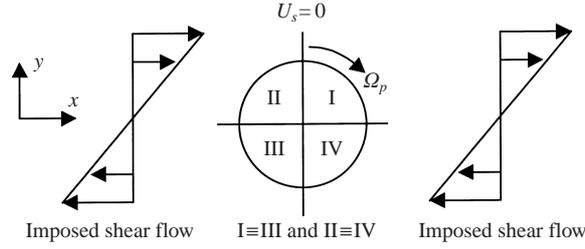
FIGURE 4. A neutrally buoyant particle in an unbounded linear shear flow.

the slip velocity of the particle (Joseph 2001)

$$U_s = \frac{\pi d^2 (\rho_p - \rho_f) g \left[ \left( 0.679 - \ln \left( \sqrt{\frac{1}{4}R} \right) \right)^2 + 0.634 \right]}{84.63 \eta} \quad \text{for a circular particle,} \\ U_s = \frac{\pi d^2 (\rho_p - \rho_f) g}{9.69 \eta \sqrt{R}} \qquad\qquad\qquad\qquad \text{for a sphere.} \right\} \quad (14)$$

The net buoyant weight on a neutrally buoyant particle ($\rho_p = \rho_f$) is zero; hence, $U_s = 0$ and from (12) and (13), $L = 0$. The Bretherton and Saffman formulae thus predict that a freely moving neutrally buoyant circular or spherical particle will have zero slip velocity in a linear shear flow in an unbounded domain. Their results are valid for particle Reynolds numbers much smaller than unity. Conversely, (12) and (13) predict that, when $R$ is small, the hydrodynamic lift on a circular or spherical particle of any density is zero when $U_s = 0$. This result can be argued from symmetry (figure 4) at any $R$.

Consider a circular particle with a zero slip velocity. The origin of the coordinate system is at the centre of the particle. In this frame, the shear flow is as in figure 4. Quadrants I and III and II and IV are symmetric with respect to origin; hence, if a lift force is up, it is also down, implying that it is zero. The same symmetry implies that the hydrodynamic drag is also zero. The argument works also for spherical particles and it is independent of the angular velocity of the particle.

The above argument was developed by Patankar & Hu and reported by Patankar (1997) in a two-dimensional numerical study of the rheology of rigid particulate mixtures in the dilute limit.

Lin, Peery & Schowalter (1970) considered flow around a rigid sphere in an unbounded linear shear flow. They assumed that $U_s = 0$ and worked matched expansions at low $R$. It is known that in the creeping flow limit the angular velocity of a freely rotating circular or spherical particle is $\frac{1}{2}\dot{\gamma}$. Lin *et al.* (1970) showed that, at a finite Reynolds number, the magnitude of angular velocity of a freely rotating particle is less than $\frac{1}{2}\dot{\gamma}$. Patankar (1997) obtained the same behaviour for a circular particle in a two-dimensional domain by performing direct numerical simulations.

At a given Reynolds number, zero slip velocity is always one solution for a neutrally buoyant circular particle freely moving in an unbounded linear shear flow, but it may not be the only solution. This solution will be unstable under certain conditions not yet understood. Sedimenting particles in high-Reynolds-number flows give rise to unsteady wakes, thus causing the particle motion to be inherently transient. Similar features of the problem of a particle in shear flows require further investigation.

Equation (14) does not predict multiple solutions for the slip velocity. Asmolov (1990) and, independently, McLaughlin (1991) generalized Saffman's analysis to
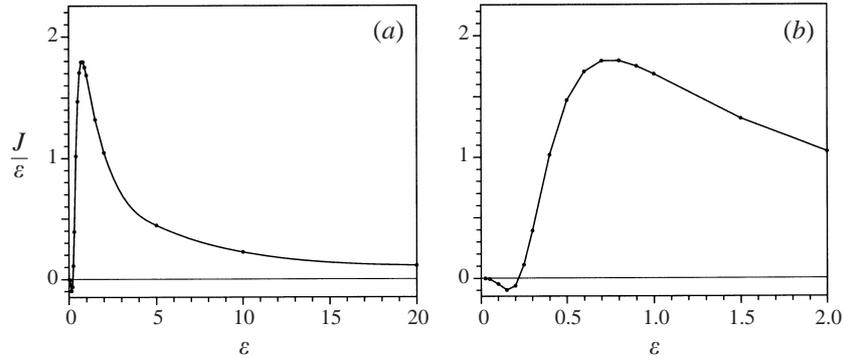
FIGURE 5. $J(\varepsilon)/\varepsilon$ *vs.* $\varepsilon$ for $\varepsilon > 0.025$. The graphs are based on McLaughlin's data for the lift on a sphere in an unbounded linear shear flow.

remove certain restrictions and derived an expression for the lift force. McLaughlin's (1991) expression for the lift force is given by

$$\left.\begin{aligned} L &= \frac{6.46}{2.255}\frac{\eta^2}{4\rho_f}R\frac{J(\varepsilon)}{\varepsilon}, \\ \varepsilon &= \frac{\sqrt{R}}{R_s}, \end{aligned}\right\} \tag{15}$$

where $J$ is a function of $\varepsilon$ only and $R_s = \rho_f U_s d/\eta$ is the slip Reynolds number. The function $J$ has a value of 2.255 as $\varepsilon \to \infty$ (the Saffman limit). Figure 5 shows the plot of $J(\varepsilon)/\varepsilon$ as a function of $\varepsilon$ (for $\varepsilon \geqslant 0.025$) based on the data provided by McLaughlin (1991). For a neutrally buoyant particle $J(\varepsilon)/\varepsilon = 0$, i.e. $\varepsilon = 0.218$ or $\varepsilon \sim \infty$ (figure 5). There is probably another value of $\varepsilon < 0.025$ at which $J(\varepsilon)/\varepsilon = 0$, but we do not have those data. Equation (15) implies $U_s = \sqrt{R}\eta/0.218\rho_f d$ or $U_s = 0$ (prediction from the Saffman formula); hence, the slip velocity is not single valued for a given $L$. The drag on the particle for each of these cases is different. The argument also works for non-neutrally buoyant particles. The two solutions from McLaughlin's equation may not both be stable.

It is of interest to compare Bretherton's formula (equation (12)) with the results of a direct simulation. Bretherton's analysis does not apply to the case of a freely moving cylinder in equilibrium under the balance of weight and lift. The condition of zero drag, required for steady motion, is not respected. Assuming some engine to move the particle with the required drag, we may compare this formula with the results from DNS.

Numerical simulations are performed in a square channel of size $W \times W$. The channel should be large enough to simulate flows in an unbounded domain. The circular particle is placed at the centre of the channel. The origin of the coordinate system is at the centre of the particle. The velocity boundary conditions are as shown in figure 6. The upper wall moves with velocity $V_1$ and the bottom wall with velocity $-V_2$. The shear rate $\dot{\gamma} = (V_1 + V_2)/W$ and the slip velocity $U_s$ is as shown in figure 6. The particle is free to rotate so that the net torque is zero at steady state.

We vary $\dot{\gamma}$ and $U_s$ in our simulations. The fluid density is $1\,\mathrm{g\,cm^{-3}}$, viscosity is 1 poise and the particle diameter is 1 cm. At $t = 0_+$ the flow is started by imposing the boundary conditions. The particle begins to rotate until a constant angular velocity is reached at steady state. The hydrodynamic lift (in the $y$-direction) and drag (in

| | $R_s = 0.003$ | | | $R_s = 0.1$ | | |
|---|---|---|---|---|---|---|
| | DNS | Analytic | % Error | DNS | Analytic | % Error |
| $R = 0.01$ { Lift | 0.00347 | 0.00449 | −22.72 | 0.08593 | 0.1496 | −42.56 |
| Drag | 0.01010 | 0.01041 | −2.98 | 0.3374 | 0.3471 | −2.79 |
| $R = 0.02$ { Lift | 0.00436 | 0.00542 | −19.56 | 0.1239 | 0.1806 | −31.39 |
| Drag | 0.01093 | 0.01145 | −4.54 | 0.3637 | 0.3818 | −4.74 |

TABLE 1. Comparison between the numerical and analytic values (equation (12)) of lift and drag per unit length (in CGS units). The error is calculated with respect to the analytic value.
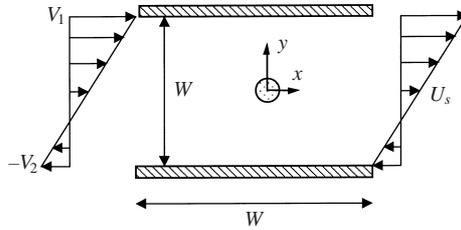


FIGURE 6. Computational domain for the simulation of linear shear flows around a circular particle.
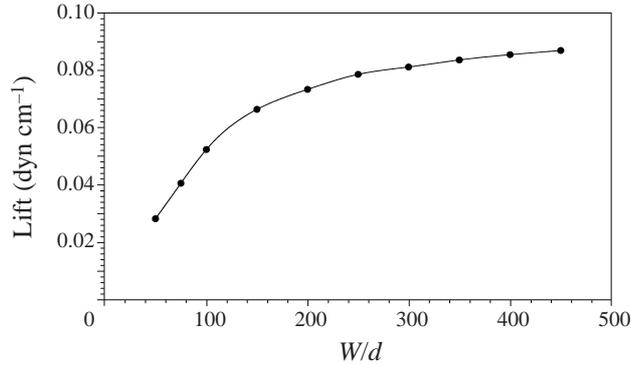


FIGURE 7. Lift *vs.* domain size for a particle in an unbounded linear shear flow.

the $x$-direction) on the particle is calculated. Figure 7 shows the plot of the lift force on the particle as a function of $W$ for $R = 0.01$ and $R_s = 0.1$. The simulations were carried out on a sequence of domains of increasing size. If this procedure is to yield a result which is asymptotically independent of the size of the domain, then the curve giving life *vs.* domain size ought to flatten out. Figure 7 shows just such a flattening. Although the curve is still rising modestly at $W = 450d$, we have used this domain for the simulations in table 1. In this table the computed values of lift and drag are compared to the analytical values from Bretherton's expressions (equation (12)). The drag force is in better agreement than the lift. Larger domains may lead to better agreements.

Joseph (2001) proposed a model problem for a planar Couette flow defined in figure 8. The circular particle of diameter $d$ is replaced by a long rectangle whose
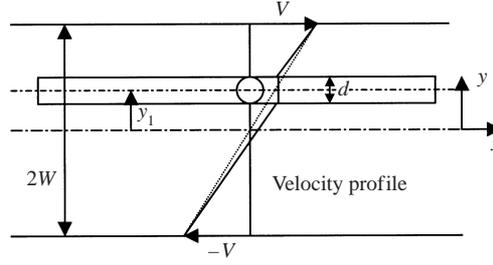
FIGURE 8. A long rectangular particle in a steady Couette flow. $\cdots$, undisturbed velocity profile; ——, velocity profile in the presence of the long particle.

short side is $d$. The rectangular particle is so long that we may neglect end effects at sections near the location of the particle centre. The mid-plane of the particle is at a distance $y_1$ from the channel centre such that $W + y_1 > \frac{1}{2}d$ and $W - y_1 > \frac{1}{2}d$. Suppose that $y = 0$ is located at the channel centre and that the channel width is $2W$. Then $u = V$ at $y = W$ and $u = -V$ at $y = -W$ and the velocity is linear. When the particle is absent

$$u = Vy/W. \tag{16}$$

In the presence of the particle, we obtain

$$\left.\begin{array}{llll} \text{for} & y_1 + \frac{1}{2}d \leqslant y \leqslant W: & u = \dfrac{V(y - \frac{1}{2}d)}{(W - \frac{1}{2}d)} & \Rightarrow \dfrac{du}{dy} = \dfrac{V}{(W - \frac{1}{2}d)}, \\[3mm] \text{for} & -W \leqslant y \leqslant y_1 - \frac{1}{2}d: & u = \dfrac{V(y + \frac{1}{2}d)}{(W - \frac{1}{2}d)} & \Rightarrow \dfrac{du}{dy} = \dfrac{V}{(W - \frac{1}{2}d)}, \\[3mm] \text{for} & y_1 - \frac{1}{2}d \leqslant y \leqslant y_1 + \frac{1}{2}d: & u = U_p \Rightarrow \dfrac{du}{dy} = 0, \end{array}\right\} \tag{17}$$

where $U_p$ is the particle velocity given by

$$U_p = \frac{Vy_1}{W - \frac{1}{2}d}. \tag{18}$$

The particle velocity is the same as the velocity in the undisturbed shear flow when $d \to 0$. The slip velcoity is

$$U_s = \frac{Vy_1}{W} - U_p = -\frac{Vy_1 d}{W(2W - d)}. \tag{19}$$

The particle leads the fluid; the slip velocity is negative when $y_1 > 0$ and positive when $y_1 < 0$. The lift is toward increasing velocity when the particle lags. It is toward decreasing velocities, toward $y = 0$, when the particle leads. The negative lift following from this line of thought leads to zero slip velocity and zero lift in a linear shear flow. When the particle is centred, the profiles in the fluid are linear and antisymmetric with respect to $y = 0$, but they are different to $Vy/W$.

The effect of particle rotation is to diminish the effect of the particle on the fluid motion. Our long particle cannot rotate, but we could express an effect of rotation by allowing for a shear profile, less than the shear in the unperturbed fluid, in the long body as if it were a very viscous fluid. The shear in the very viscous fluid would be greater than the zero shear of the solid and less than the shear in the undisturbed flow. The difference between the shear in the undisturbed fluid and the very viscous
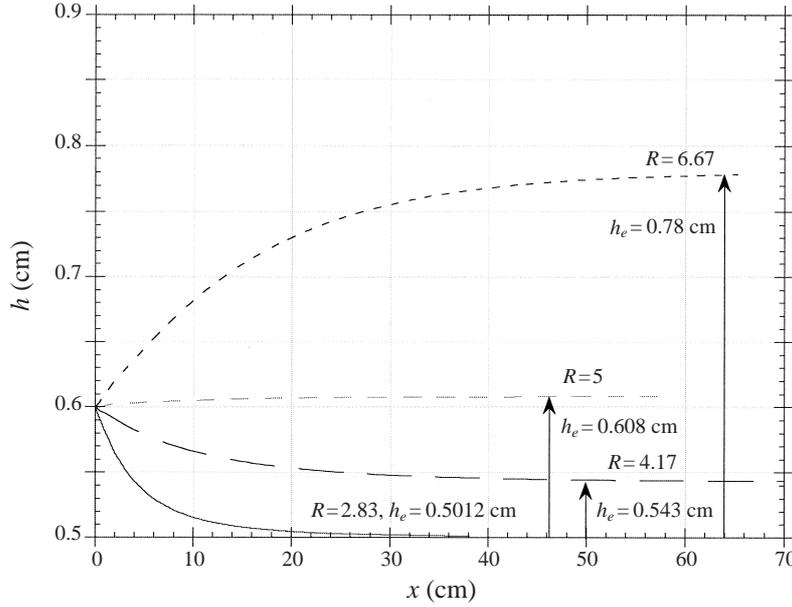
FIGURE 9. Cross-stream migration of a single particle ($\rho_p > \rho_f$). A single particle of diameter 1 cm is released at a height of 0.6$d$ in a Poiseuille flow. It migrates to an equilibrium height $h_e$.

fluid can be viewed as representing the angular slip velocity. The 'no shear' solid corresponds to a circular particle for which the rotation is suppressed.

## 4. Lift-off of a single particle in plane Poiseuille flows of a Newtonian fluid

In figure 9 we plot the trajectory of the circular particle as a function of the distance travelled along the axial direction. The channel dimensions are: $W/d = 12$ and $l/d = 22$, where $d = 1$ cm (figure 1). The fluid density and viscosity are $1 \, \mathrm{g \, cm^{-3}}$ and 1 poise, respectively. The particle density is $1.01 \, \mathrm{g \, cm^{-3}}$ and $R_G = 9.81$. The centre of the particle is initially at $y = 0.6d$. When $R < 2.83$, the particle falls to the bottom wall. For $R > 2.83$, it falls or rises to an equilibrium height $h_e$ at which the buoyant weight balances the hydrodynamic lift. Thus, the critical value of $R$ for lift-off in this case is 2.83. The equilibrium height increases with $R$ (figure 9).

A rearrangement of equation (9) implies that the non-dimensional equilibrium height, $h_e/d$, is a function of $R$, $R_G$ and $W/d$. Figure 10($a$) shows the plot of $h_e/d$ as a function of $R$ at different values of $R_G$ with $W/d = 12$. The equilibrium height increases as the shear Reynolds number is increased at all values of $R_G$. A larger shear Reynolds number is required to lift a heavier particle to a given equilibrium height. Figure 10($b$) compares the equilibrium height of a particle of given density in channels of different widths ($W/d = 12$, 24 and 48). $l/d = 44$ for a channel with $W/d = 24$, whereas $l/d = 88$ for $W/d = 48$. At a given shear Reynolds number the dimensionless equilibrium height is larger for the bigger channel. This is probably due to the difference in the curvature of the velocity profile.

The critical shear Reynolds number for lift-off is a function of $R_G$ (or $G$) and $W/d$ (equation (9)). In our numerical simulations, the gap between the particle and the wall can never be zero (Hu & Patankar 2001). The smallest allowable gap size is set to be 0.0005$d$. The smallest shear Reynolds number at which we observe an

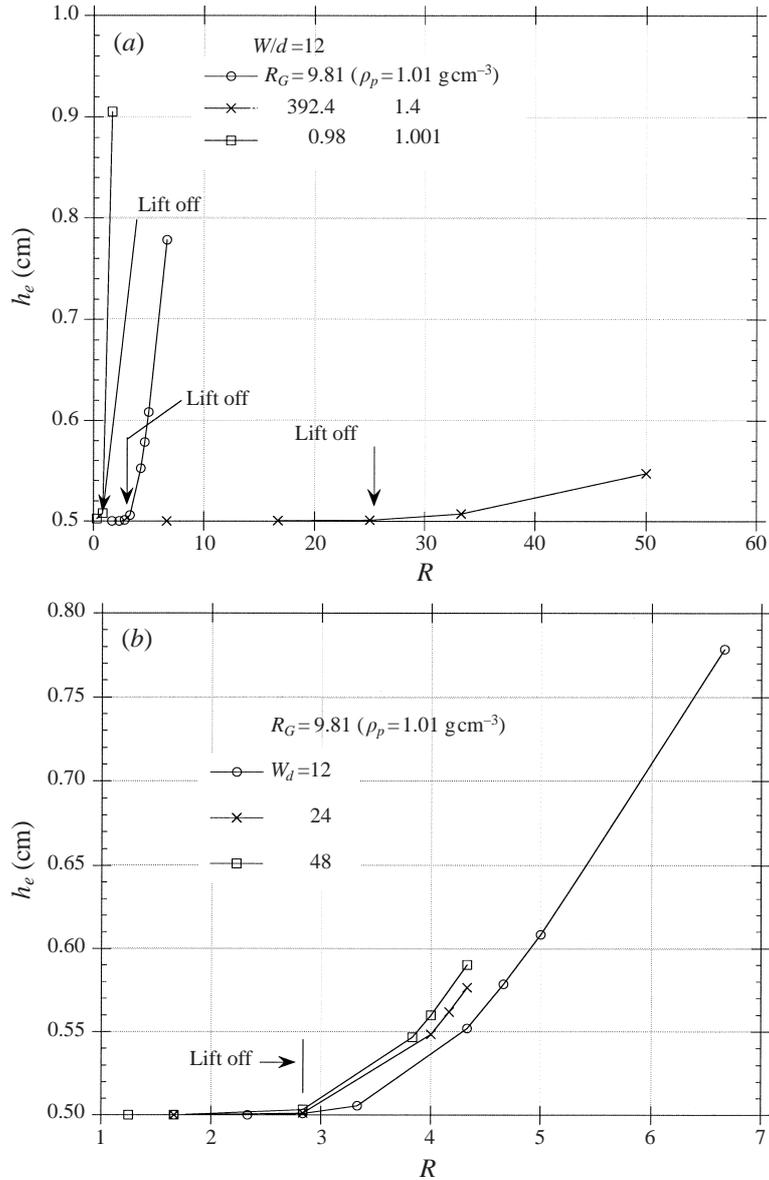FIGURE 10. (a) Lift-off and equilibrium height as a function of the shear Reynolds number at different values of $R_G$. (b) Equilibrium height vs. shear Reynolds number at different channel widths.

equilibrium height greater than $0.5005d$ is therefore identified as the critical shear Reynolds number for lift-off in our dynamic simulations. In most cases, the smallest equilibrium height we obtain is around $0.501d$. To obtain a correlation between $R_G$ and $R$ at the critical condition for lift-off, we simulate the motion in a periodic channel in which the particle is free to rotate and translate in the axial ($x$-) direction. The height of the particle centre from the bottom wall of the channel is fixed at $0.501d$. There is no external body force in the axial direction and no external torque is applied. Simulations are performed at different values of the shear Reynolds number and channel widths. The hydrodynamic lift force $L$ on the particle is calculated. For
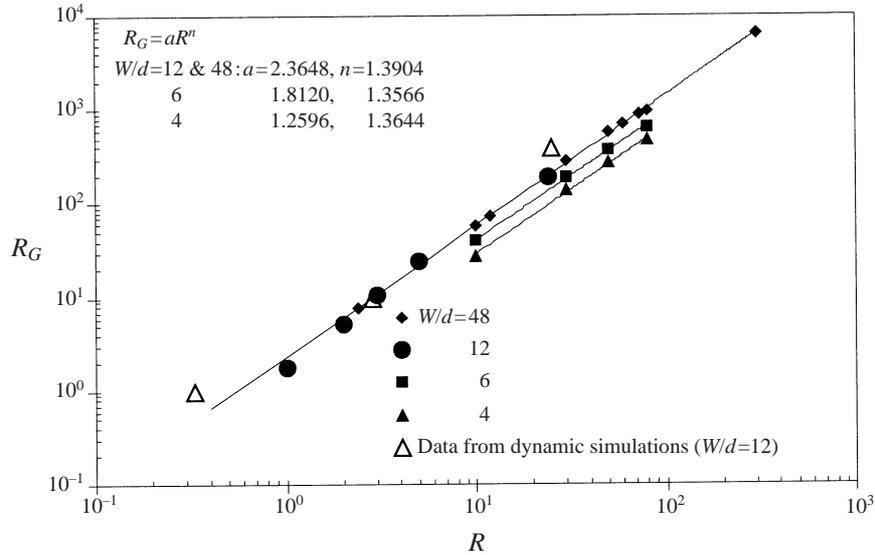
FIGURE 11. The plot of $R_G$ *vs.* the critical shear Reynolds number $R$ for lift-off on a logarithmic scale at different values of $W/d$.
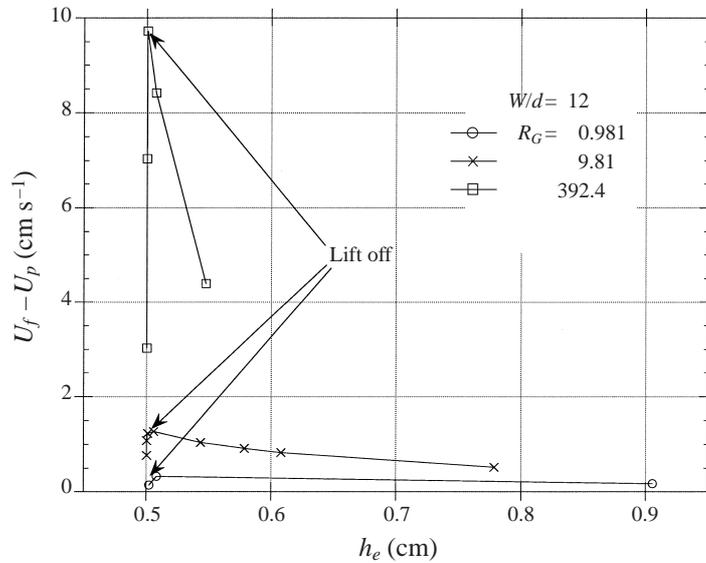


FIGURE 12. Slip velocity *vs.* equilibrium height for different particle densities.

a particle in equilibrium, $R_G = \rho_f(\rho_s - \rho_f)gd^3/\eta^2 = 4\rho_f Ld/\pi\eta^2$. Figure 11 shows the plot of $R_G$ *vs.* the critical shear Reynolds number for lift-off at different values of $W/d$. It is seen that larger $R$ is required to lift a heavier particle. We observe that the critical shear Reynolds number for the lift-off of a given particle increases as the channel width decreases for $W/d < 12$. There is no effect of the channel width on the critical shear Reynolds number for $W/d > 12$ (figures 10(*b*) and 11). The data from the simulations can be represented by a power law equation given by $R_G = aR^n$, where the values of $a$ and $n$ are given in figure 11.
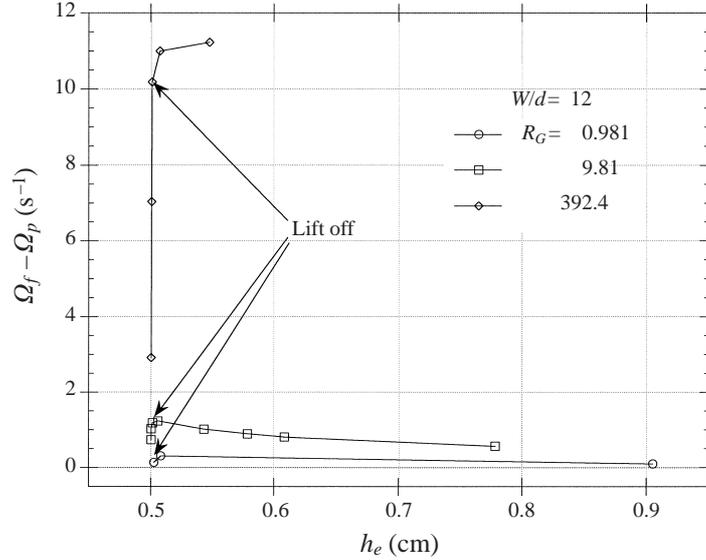
FIGURE 13. Slip angular velocity *vs.* equilibrium height for different particle densities.

$U_p$ and $\Omega_p$ are the translational and angular velocities, respectively, of the particle in equilibrium (figure 3). The hydrodynamic drag and torque on the particle is zero. In figure 12 we plot the dynamic simulations results of the slip velocity, $U_f - U_p$, *vs.* the equilibrium height for particles of different densities. A similar plot for the slip angular velocity, $\frac{1}{2}\dot{\gamma} - \Omega_p$, is shown in figure 13. We observe that a larger slip velocity is required at a given equilibrium height to balance a heavier particle.

All the computed values of $R_G, R/G, R, \bar{p}, h_e, U_p, U_f, U_s = U_f - U_p, \Omega_p, \Omega_f = \frac{1}{2}\dot{\gamma}$ and $\Omega_s = \frac{1}{2}\dot{\gamma} - \Omega_p$ at equilibrium are given in table 2, where $U_f$ and $\dot{\gamma}$ are as shown in figure 3. These quantities define a data structure generated by DNS which can help in the creation and validation of lift models; the tables give the answers to which the models aspire.

Choi & Joseph (2001) performed simulations for single-particle lift-off in Poiseuille flows at much higher shear Reynolds numbers. They observed that the rise and other equilibrium properties are not smooth functions of $R$. They found the existence of multiple steady states and hysteresis. Figure 14 shows the plot of $h_e/d$ *vs.* $R$ at different values of angular velocity of the particle. The particle density is $1.01\,\mathrm{g\,cm^{-3}}$, $W/d = 12$, $l/d = 22$, $\eta = 1$ poise, $d = 1\,\mathrm{cm}$ and $\rho_f = 1\,\mathrm{g\,cm^{-3}}$. The particle is initially placed close to the bottom wall. Simulations were performed in a periodic channel with three different conditions on the angular motion of the particle: zero hydrodynamic torque (free rotation), zero angular velocity ($\Omega_p = 0$) and zero slip angular velocity ($\Omega_s = 0$). In each of these cases, the equilibrium height shows a sharp rise after a critical shear Reynolds number that is smallest for a non-rotating particle and is largest when the slip angular velocity is suppressed. The sharp rise or 'jump' in the equilibrium height can be explained in terms of turning-point bifurcation to be discussed in §6. Choi & Joseph (2001) reported the freely rotating case shown in figure 14. The angular velocity of the particle is seen to have little effect on the equilibrium height before the 'jump'. The greater the slip angular velocity, the higher the particle rises after the 'jump'. Models for lift should account for this effect of the slip angular velocity.

| $R/G$ | $R_G$ | $R$ | $\bar{p}$ | $h_e$ | $U_p$ | $U_f$ | $U_s$ | $\Omega_p$ | $\Omega_f$ | $\Omega_s$ |
|---|---|---|---|---|---|---|---|---|---|---|
| *(a)* | | | | | | | | | | |
| **0.1133** | **0.981** | **0.3333** | **0.0555** | **0.5024** | **0.0170** | **0.1605** | **0.1436** | **0.0161** | **0.1527** | **0.1367** |
| 0.7079 | 0.981 | 0.8333 | 0.1389 | 0.5081 | 0.0820 | 0.4055 | 0.3235 | 0.0752 | 0.3814 | 0.3062 |
| 2.8316 | 0.981 | 1.6667 | 0.2778 | 0.9055 | 1.2310 | 1.3953 | 0.1643 | 0.6085 | 0.7076 | 0.0991 |
| **0.8183** | **9.81** | **2.8333** | **0.4722** | **0.5012** | **0.1337** | **1.3608** | **1.2271** | **0.1147** | **1.2983** | **1.1836** |
| 1.1326 | 9.81 | 3.3333 | 0.5556 | 0.5058 | 0.3479 | 1.6149 | 1.2670 | 0.2934 | 1.5262 | 1.2328 |
| 1.7697 | 9.81 | 4.1667 | 0.6944 | 0.5433 | 1.1230 | 2.1613 | 1.0383 | 0.8868 | 1.8947 | 1.0079 |
| 2.2200 | 9.81 | 4.6667 | 0.7778 | 0.5786 | 1.6560 | 2.5699 | 0.9139 | 1.2220 | 2.1083 | 0.8863 |
| 2.5484 | 9.81 | 5.0000 | 0.8333 | 0.6083 | 2.0590 | 2.8873 | 0.8283 | 1.4430 | 2.2465 | 0.8035 |
| 4.5305 | 9.81 | 6.6667 | 1.1111 | 0.7784 | 4.3350 | 4.8527 | 0.5177 | 2.3340 | 2.9009 | 0.5669 |
| **1.5928** | **392.4** | **25.000** | **4.1667** | **0.5009** | **2.2820** | **11.999** | **9.7178** | **1.2790** | **11.456** | **10.177** |
| 2.8316 | 392.4 | 33.333 | 5.5556 | 0.5074 | 7.7790 | 16.198 | 8.4192 | 4.2600 | 15.257 | 10.997 |
| 6.3710 | 392.4 | 50.000 | 8.3333 | 0.5475 | 21.730 | 26.126 | 4.3960 | 11.500 | 22.719 | 11.219 |
| *(b)* | | | | | | | | | | |
| **0.8183** | **9.81** | **2.8333** | **0.2361** | **0.5015** | **0.1611** | **1.3912** | **1.2301** | **0.1381** | **1.3575** | **1.2194** |
| 1.6310 | 9.81 | 4.0000 | 0.3333 | 0.5485 | 1.2020 | 2.1439 | 0.9419 | 0.9468 | 1.9086 | 0.9618 |
| 1.7697 | 9.81 | 4.1667 | 0.3472 | 0.5619 | 1.3990 | 2.2864 | 0.8874 | 1.0750 | 1.9858 | 0.9108 |
| 1.9141 | 9.81 | 4.3333 | 0.3611 | 0.5766 | 1.6030 | 2.4386 | 0.8356 | 1.2010 | 2.0626 | 0.8616 |
| *(c)* | | | | | | | | | | |
| **0.8183** | **9.81** | **2.8333** | **0.1181** | **0.5034** | **0.2491** | **1.4113** | **1.1622** | **0.2134** | **1.3870** | **1.1736** |
| 1.4979 | 9.81 | 3.8333 | 0.1597 | 0.5467 | 1.1640 | 2.0718 | 0.9078 | 0.9247 | 1.8730 | 0.9483 |
| 1.6310 | 9.81 | 4.0000 | 0.1667 | 0.5600 | 1.3590 | 2.2139 | 0.8549 | 1.0540 | 1.9533 | 0.8993 |
| 1.9141 | 9.81 | 4.3333 | 0.1806 | 0.5901 | 1.7750 | 2.5257 | 0.7507 | 1.3070 | 2.1134 | 0.8064 |

TABLE 2. Data structure for a freely translating and rotating circular particle levitated by Poiseuille flow ($d = 1\,\text{cm}$, $\rho_f = 1\,\text{g cm}^{-3}$ and $\eta = 1$ poise). Bold numbers represent the critical condition for lift-off. All the dimensional variables are given in CGS units. (*a*) $W/d = 12$, $l/d = 22$, (*b*) $W/d = 24$, $l/d = 44$, (*c*) $W/d = 48$, $l/d = 88$.



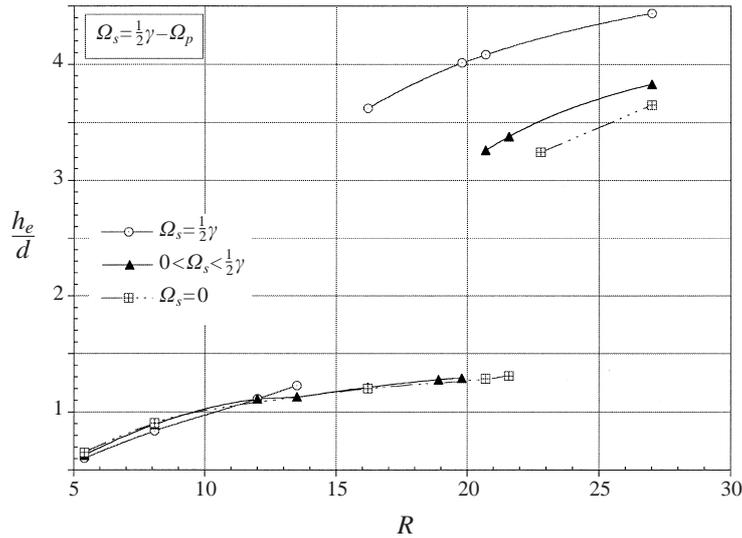FIGURE 14. Lift-off of a circular particle from a horizontal wall in a Poiseuille flow of a Newtonian fluid ($W/d = 12$, $l/d = 22$, $\eta = 1$ poise, $d = 1\,\text{cm}$, $\rho_p = 1.01\,\text{g cm}^{-3}$).
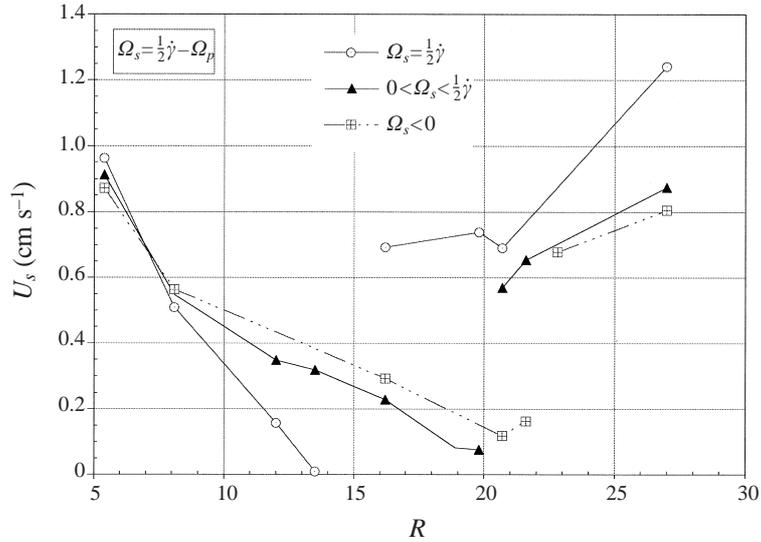
FIGURE 15. Slip velocity *vs.* shear Reynolds number for the cases depicted in figure 14.
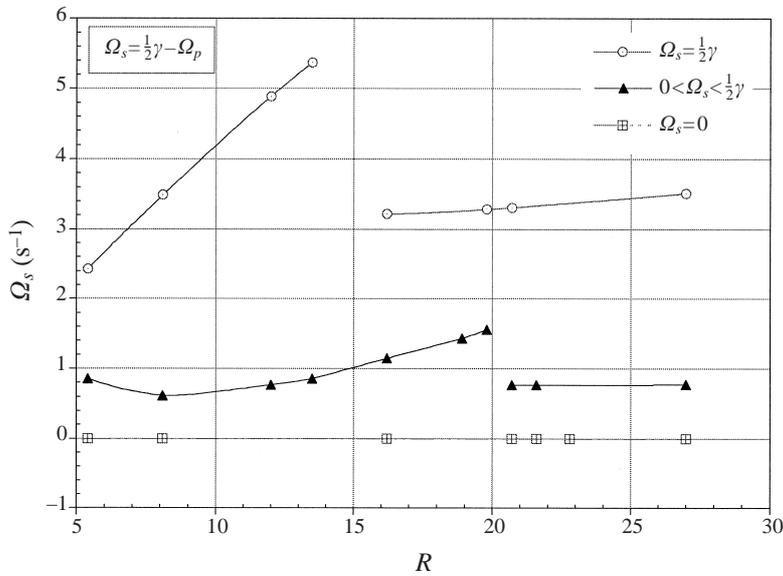


FIGURE 16. Slip angular velocity *vs.* Reynolds number for the cases depicted in figure 14.

Figure 15 shows the plot of slip velocity *vs.* $R$ for this case. It is seen that the slip velocity decreases before the 'jump' and increases sharply at the 'jump'. The slip velocity does not show a consistent trend with respect to the angular velocity of the particle. The slip angular velocity also shows a sharp change at the 'jump' (figure 16). As expected, the slip angular velocity is maximum for a non-rotating particle.

In figure 17 we plot the rise of a neutrally buoyant particle to the equilibrium height as a function of time for $W/d = 12$, $l/d = 22$, $d = 1$ cm, $\eta = 1$ poise, $\rho_f = 1$ g cm$^{-3}$ and $R = 5.4$. The simulations are performed in a periodic channel. We compare the rise of freely rotating and non-rotating particles. A neutrally buoyant
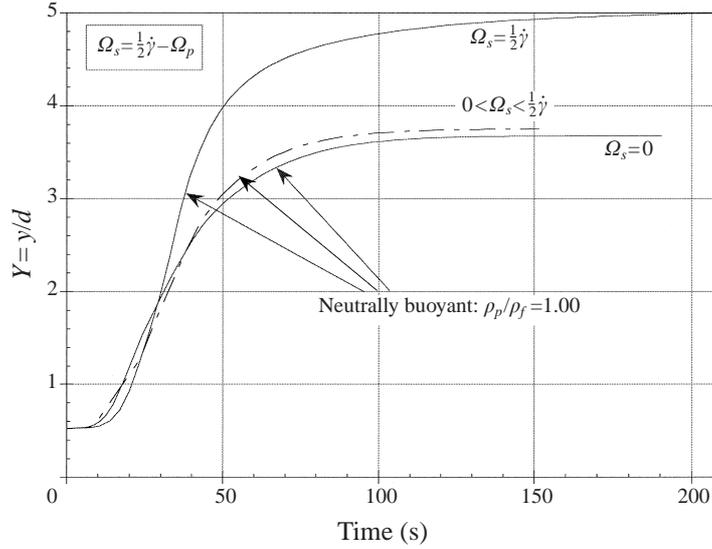
FIGURE 17. Rise *vs.* time for a neutrally buoyant particle ($R = 5.4$, $W/d = 12$, $l/d = 22$, $\eta = 1$ poise, $d = 1$ cm).

freely rotating particle rises to a Segré–Silberberg radius; the non-rotating one rises more. Our results are in qualitative agreement with the experimental results of Segré & Silberberg (1961, 1962). A smaller lift is obtained when the slip angular velocity is entirely suppressed ($\Omega_s = 0$) but the particle does rise. The greater the slip angular velocity the higher the particle rises.

Table 3 gives data for the results presented in figures 14–17. In the next section we discuss the contribution to the hydrodynamic lift force from pressure and shear stress in a Newtonian fluid.

## 5. Lift due to pressure and shear on a particle in plane Poiseuille flows of a Newtonian fluid

Numerical simulation can be used to analyse the forces which enter into the lift balance

$$\left.\begin{array}{l} L_p + L_s = \frac{1}{4}\pi d^2(\rho_p - \rho_f)g, \\[2mm] L_p = \displaystyle\oint_{\partial P} -p\boldsymbol{n}\,\mathrm{d}\Gamma, \\[2mm] L_s = \displaystyle\oint_{\partial P} \eta\boldsymbol{A}\cdot\boldsymbol{n}\,\mathrm{d}\Gamma, \end{array}\right\} \tag{20}$$

where the buoyant weight is balanced by the sum of the pressure lift $L_p$ and the shear lift $L_s$. It is well known that only the tangential (or shear) component of $\boldsymbol{A}\cdot\boldsymbol{n}$ is non-zero on a rigid surface. We define lift fractions

$$\Phi_p = \frac{L_p}{L_p + L_s}, \quad \Phi_s = \frac{L_s}{L_p + L_s}, \quad \Phi_p + \Phi_s = 1. \tag{21}$$

In figure 18 we plot the lift fraction *vs.* R for cases shown in figure 10(*a*). The figure shows that the pressure lift is greater than the shear lift and that the pressure lift

| $R/G$ | $R_G$ | $R$ | $\bar{p}$ | $h_e$ | $U_p$ | $U_f$ | $U_s$ | $\Omega_p$ | $\Omega_f$ | $\Omega_s$ |
|---|---|---|---|---|---|---|---|---|---|---|
| 2.9725 | 9.81 | 5.40 | 0.90 | 0.6020 | 2.1250 | 3.0877 | 0.9627 | 0.0000 | 2.4291 | 2.4291 |
| 6.6881 | 9.81 | 8.10 | 1.35 | 0.8366 | 5.7950 | 6.3040 | 0.5090 | 0.0000 | 3.4853 | 3.4853 |
| 14.679 | 9.81 | 12.00 | 2.00 | 1.1130 | 11.960 | 12.117 | 0.1572 | 0.0000 | 4.8870 | 4.8870 |
| 18.578 | 9.81 | 13.50 | 2.25 | 1.2260 | 14.870 | 14.860 | 0.0100 | 0.0000 | 5.3708 | 5.3708 |
| 26.752 | 9.81 | 16.20 | 2.70 | 3.6200 | 40.260 | 40.953 | 0.6930 | 0.0000 | 3.2130 | 3.2130 |
| 39.963 | 9.81 | 19.80 | 3.30 | 4.0120 | 52.140 | 52.879 | 0.7389 | 0.0000 | 3.2802 | 3.2802 |
| 43.679 | 9.81 | 20.70 | 3.45 | 4.0830 | 55.070 | 55.761 | 0.6908 | 0.0000 | 3.3068 | 3.3068 |
| 74.312 | 9.81 | 27.00 | 4.50 | 4.4410 | 74.290 | 75.531 | 1.2414 | 0.0000 | 3.5077 | 3.5077 |
| **2.9725** | **9.81** | **5.40** | **0.90** | **0.6268** | **2.2960** | **3.2079** | **0.9119** | **1.5600** | **2.4180** | **0.8579** |
| **6.6881** | **9.81** | **8.10** | **1.35** | **0.8923** | **6.1420** | **6.6902** | **0.5482** | **2.8330** | **3.4477** | **0.6147** |
| **14.679** | **9.81** | **12.00** | **2.00** | **1.1100** | **11.740** | **12.088** | **0.3479** | **4.1220** | **4.8900** | **0.7680** |
| **18.578** | **9.81** | **13.50** | **2.25** | **1.1300** | **13.500** | **13.818** | **0.3185** | **4.6240** | **5.4787** | **0.8548** |
| **26.752** | **9.81** | **16.20** | **2.70** | **1.2110** | **17.410** | **17.638** | **0.2284** | **5.3200** | **6.4652** | **1.1452** |
| **36.413** | **9.81** | **18.90** | **3.15** | **1.2760** | **21.470** | **21.552** | **0.0820** | **6.0080** | **7.4403** | **1.4323** |
| **39.963** | **9.81** | **19.80** | **3.30** | **1.2900** | **22.720** | **22.796** | **0.0762** | **6.2140** | **7.7715** | **1.5575** |
| **43.679** | **9.81** | **20.70** | **3.45** | **3.2610** | **48.590** | **49.159** | **0.5688** | **3.9550** | **4.7248** | **0.7698** |
| **47.560** | **9.81** | **21.60** | **3.60** | **3.3800** | **51.790** | **52.444** | **0.6540** | **3.9490** | **4.7160** | **0.7670** |
| **74.312** | **9.81** | **27.00** | **4.50** | **3.8310** | **69.540** | **70.415** | **0.8747** | **4.1040** | **4.8803** | **0.7763** |
| 2.9725 | 9.81 | 5.40 | 0.90 | 0.6511 | 2.4530 | 3.3252 | 0.8722 | 2.4070 | 2.4070 | 0.0000 |
| 6.6881 | 9.81 | 8.10 | 1.35 | 0.9047 | 6.2120 | 6.7756 | 0.5636 | 3.4390 | 3.4393 | 0.0000 |
| 26.752 | 9.81 | 16.20 | 2.70 | 1.1990 | 17.190 | 17.483 | 0.2930 | 6.4810 | 6.4814 | 0.0000 |
| 43.679 | 9.81 | 20.70 | 3.45 | 1.2830 | 23.600 | 23.719 | 0.1186 | 8.1360 | 8.1368 | 0.0000 |
| 47.560 | 9.81 | 21.60 | 3.60 | 1.3080 | 25.010 | 25.173 | 0.1632 | 8.4460 | 8.4456 | 0.0000 |
| 52.991 | 9.81 | 22.80 | 3.80 | 3.2440 | 53.290 | 53.968 | 0.6784 | 5.2370 | 5.2364 | 0.0000 |
| 74.312 | 9.81 | 27.00 | 4.50 | 3.6520 | 67.790 | 68.595 | 0.8054 | 5.2830 | 5.2830 | 0.0000 |
| $\infty$ | 0 | 5.4 | 0.90 | 4.9999 | 15.670 | 15.749 | 0.0800 | 0.0000 | 0.4500 | 0.4500 |
| $\infty$ | **0** | **5.4** | **0.90** | **3.7530** | **13.780** | **13.928** | **0.1480** | **0.9580** | **1.0110** | **0.0530** |
| $\infty$ | 0 | 5.4 | 0.90 | 3.6810 | 13.630 | 13.780 | 0.1500 | 1.0440 | 1.0440 | 0.0000 |

TABLE 3. Data structure for a freely translating circular particle levitated by Poiseuille flow ($W/d = 12$; $l/d = 22$, $d = 1\,\text{cm}$, $\rho_f = 1\,\text{g}\,\text{cm}^{-3}$ and $\eta = 1$ poise). Bold numbers are for freely rotating particles. All the dimensional variables are given in CGS units.

fraction is greater for heavy particles. Figure 19 shows the plot of lift fraction *vs. R* for cases in figure 14. For a freely rotating particle, the pressure lift is higher than the shear lift at lower shear Reynolds numbers but after the 'jump' they are of the same order. A non-rotating particle always has a greater contribution to lift from pressure.

Figure 20 shows the pressure and the viscous shear stress distributions around the particle at different shear Reynolds numbers and particle rotations. The particle velocity lags the undisturbed fluid velocity (figure 21). The curvature of the undisturbed velocity profile creates a higher velocity of the fluid relative to the particle on the bottom half (figure 21). This was recognized by Feng *et al.* (1994). The stronger relative flow on the bottom half results in a larger viscous shear stress at the bottom, i.e. at $\theta = 180°$ (figures 20*a*, 20*b* and 20*e*).

Figure 21 shows the streamlines around the particle. The fluid velocity incident on the bottom half gives rise to the high pressure $P_1$ (in the third quadrant) that pushes the particle up. The incident fluid moves up, as shown by the streamline in figure 21, giving rise to the viscous shear stress $S_1$ at $\theta = 270°$ in the upward direction. Similarly, pressure and shear forces, $P_2$ and $S_2$, respectively, act on the particle owing to the velocity incident on the top half as shown in figure 21. Since the incident velocity on the bottom half is more, the lift due to $P_1$ and $S_1$ dominates, giving rise to a net upward force on the particle. This is consistent with the observations in figures 20(*c*),
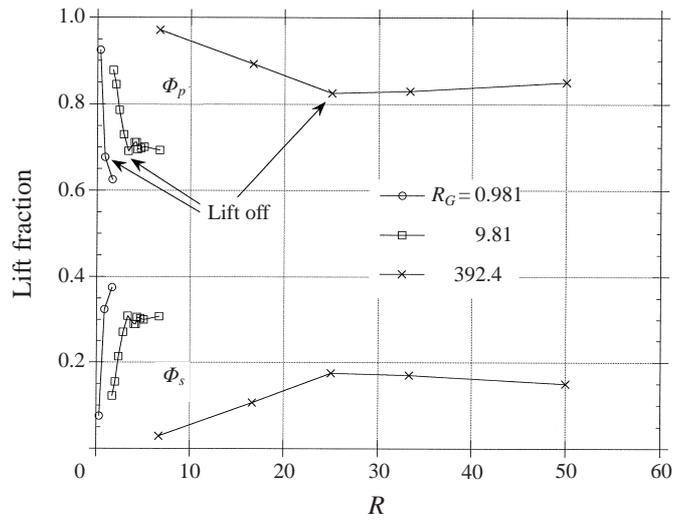
FIGURE 18. Lift fractions due to the pressure and the viscous shear stress ($W/d = 12$).
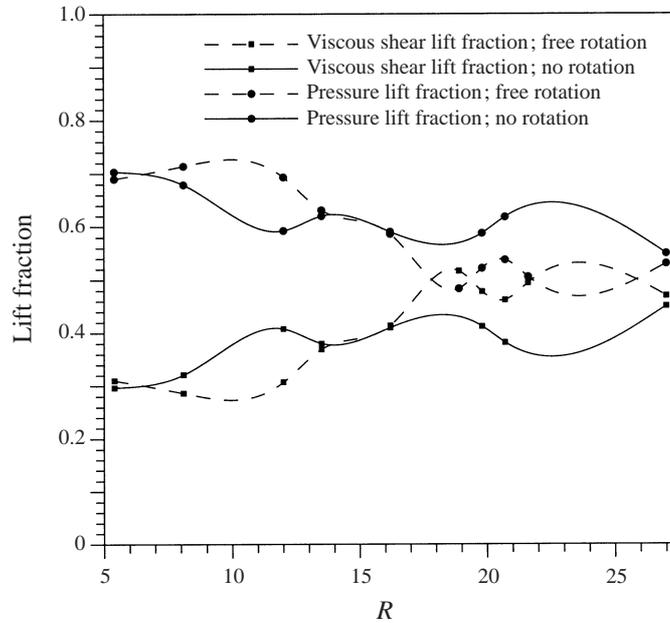The pressure lift dominates.

FIGURE 19. Lift fraction *vs.* shear Reynolds number for the cases shown in figure 14.
Lift fractions for a freely rotating and a non-rotating particle are shown.

$20(d)$ and $20(f)$. The regions of low pressure on the particle surface are seen to be
less important in determining the lift on the particle as compared to the regions of
high pressure.

The viscous shear stresses near $\theta = 90°$ and $\theta = 270°$ are smaller for a non-rotating
particle. We see from figure 21 that the magnitudes of $S_1$ and $S_2$ would decrease for
a non-rotating particle owing to smaller relative velocities between the fluid and the
particle surface at $\theta = 90°$ and $\theta = 270°$. The plot of viscous shear stress distribution
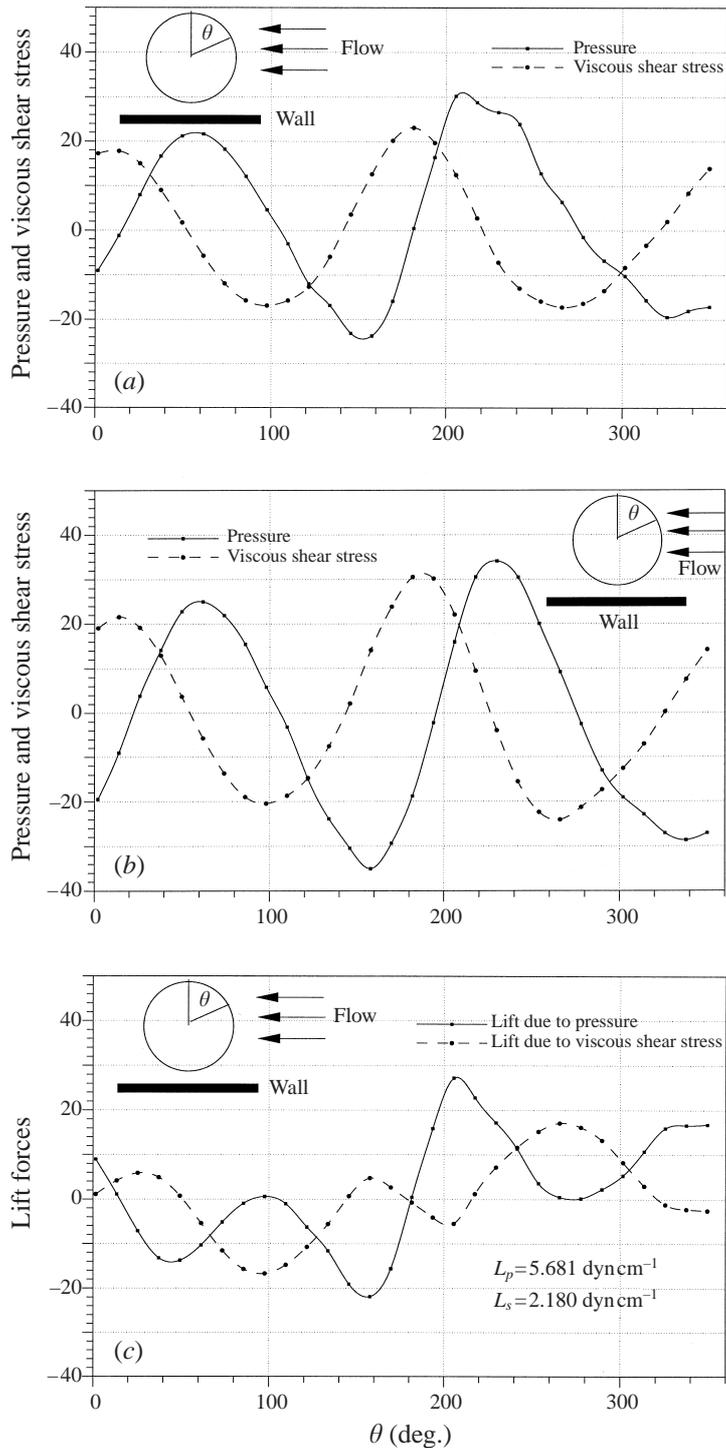
FIGURE 20. (*a*) Distributions of pressure and viscous shear stress on the surface of a freely rotating circular particle in a Poiseuille flow of a Newtonian fluid ($W/d = 12$, $l/d = 22$, $d = 1$ 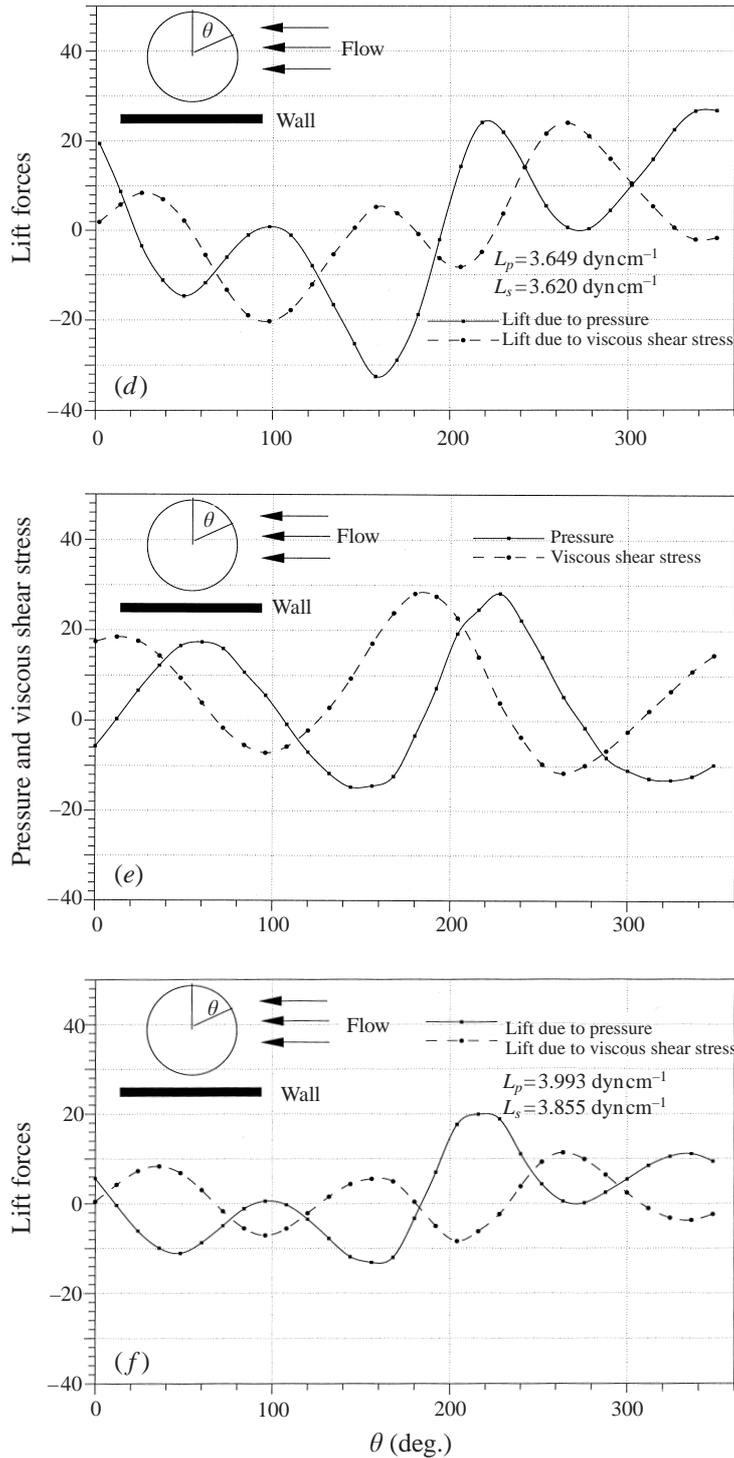cm, $\rho_p/\rho_f = 1.01$, $R = 8.1$ (before bifurcation)). (*b*) Distributions of pressure and viscous shear stress on the surface of a freely rotating circular particle in a Poiseuille flow of a Newtonian fluid ($W/d = 12$, $l/d = 22$, $d = 1$ cm, $\rho_p/\rho_f = 1.01$, $R = 27$ (after bifurcation)). (*c*) The distributions of lift forces on the surface of a freely rotating circular particle in a Poiseuille flow of a Newtonian fluid ($W/d = 12$, $l/d = 22$, $d = 1$ cm, $\rho_p/\rho_f = 1.01$, $R = 8.1$ (before bifurcation)).

FIGURE 20 (continued). (*d*) The distributions of lift forces on the surface of a freely rotating circular particle in a Poiseuille flow of a Newtonian fluid ($W/d = 12$, $l/d = 22$, $d = 1$ cm, $\rho_p/\rho_f = 1.01$, $R = 27$ (after bifurcation)). (*e*) Distributions of pressure and viscous shear stress on the surface of a non-rotating rotating circular particle in a Poiseuille flow of a Newtonian fluid ($W/d = 12$, $l/d = 22$, $d = 1$ cm, $\rho_p/\rho_f = 1.01$, $R = 27$ (after bifurcation)). (*f*) The distributions of lift forces on the surface of a non-rotating rotating circular particle in a poiseuille flow of a Newtonian fluid ($W/d = 12$, $l/d = 22$, $d = 1$ cm, $\rho_p/\rho_f = 1.01$, $R = 27$ (after bifurcation)).
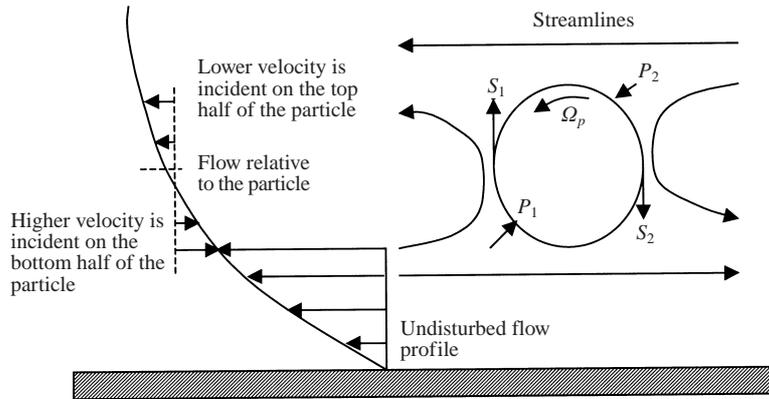
FIGURE 21. Cartoon depicting the fluid velocity and the streamlines relative to a particle in a plane Poiseuille flow. The fluid approaches the particle with a higher velocity in the bottom half of the particle. Consequently, the pressure $P_1$ (in bold) is greater than $P_2$ and the viscous shear stress $S_1$ (in bold) is greater than $S_2$.

is therefore shifted in the positive direction for a non-rotating particle (figure 20$e$) giving a greater lift as compared to a freely rotating particle at the same equilibrium height; a non-rotating particle is seen to rise more.

The above observations are similar to those reported by Zhu (2000) for the lift-off of a particle in a simple shear (Couette) flow, where they reported that the shear stress and pressure on the particle surface both contribute to the lift force owing to the inertia effects.

## 6. Turning-point bifurcation of the equilibrium position in the lift-off of a particle in plane Poiseuille flows

We study the turning-point bifurcation phenomenon by performing two-dimensional simulations of the motion of a circular particle in plane Poiseuille flows. The motion is simulated in a periodic channel in which the particle is free to rotate and translate in the axial ($x$-) direction. The height of the particle centre from the bottom wall of the channel is fixed so that it does not translate in the transverse direction. There is no external body force in the axial direction and no external torque is applied. Gravity acts in the negative $y$-direction. The particle is initially at rest and eventually reaches a state of steady motion.

At steady state, the particle translates in the axial direction at a constant velocity and rotates at a constant angular velocity. At the prescribed height, these velocities are such that there is no net hydrodynamic drag or torque. The flow field at steady state is independent of the particle density since the particle acceleration is zero (equation (5)). Only the axial and angular motion equations of the particle are solved in our simulations. The steady-state translational and angular velocities, as well as the hydrodynamic lift force, are independent of the particle densities used in our simulations. This has been confirmed from our numerical results.

The hydrodynamic lift force $L$ on the particle in the transverse direction depends on the height of the particle and the shear Reynolds number for a Newtonian suspending fluid and given channel and particle dimensions. We can select a particle of density
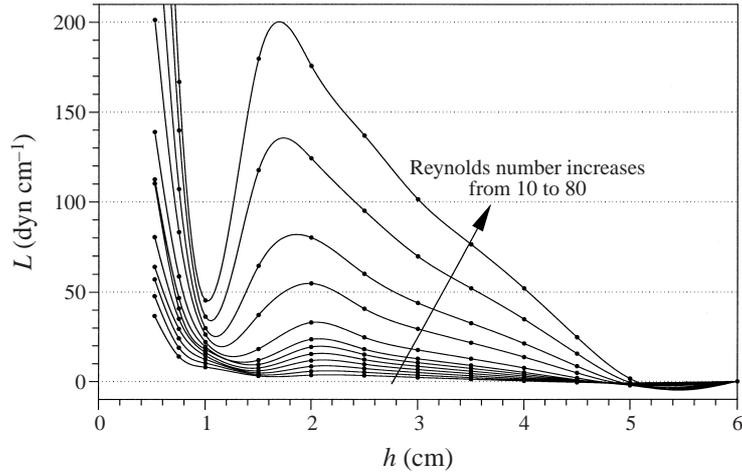
FIGURE 22. The hydrodynamic lift force on the particle as a function of the height of its centre from the bottom wall at different shear Reynolds numbers. $h = 0$ cm is the bottom wall and $h = 6$ cm is the channel centreline.
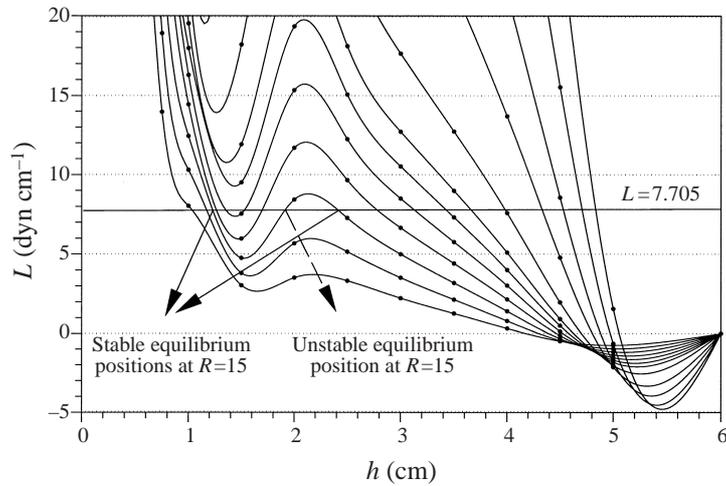


FIGURE 23. Finding the equilibrium height of a particle of given density at different values of shear Reynolds number.

$\rho_p$ given by

$$\rho_p = \rho_f + \frac{L}{V_p g}, \tag{22}$$

such that the lift just balances the buoyant weight.

Figure 22 shows the plot $L$ as a function of the height of its centre at different values of shear Reynolds number. The suspending fluid is Newtonian, $l/d = 22$, $W/d = 12$ and $d = 1$ cm. The fluid density is $1\,\mathrm{g\,cm^{-3}}$ and its viscosity is 1 poise. This plot can be used to find the equilibrium height of a particle of given density at different values of $R$.

A particle of density $\rho_p$ will be in equilibrium at a height where $L = (\rho_p - \rho_f)gV_p$. As an example, we consider a particle of density $1.01\,\mathrm{g\,cm^{-3}}$. This particle will be
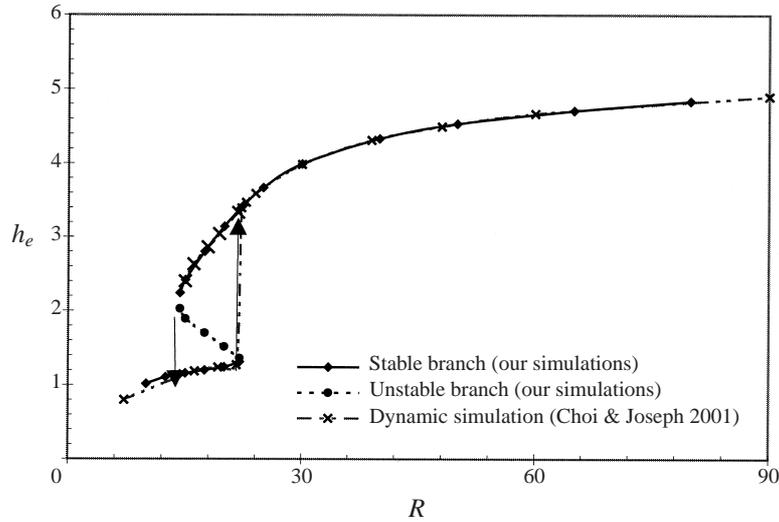
FIGURE 24. Equilibrium height as a function of shear Reynolds number for a
particle of density $1.01\,\mathrm{g\,cm^{-3}}$.

in equilibrium when $L = 7.705\,\mathrm{dyn\,cm^{-1}}$. The equilibrium heights at a given shear
Reynolds number are identified as the points of intersection between the curve of $L$
vs. $h$ and $L = 7.705$ in figure 23. The intersection points where the slope of the $L$ vs. $h$
curve is positive are unstable equilibrium points, whereas a negative slope represents
a stable equilibrium point (figure 23). Figure 24 shows the plot of the equilibrium
height of the particle of density $1.01\,\mathrm{g\,cm^{-3}}$ vs. $R$. We reproduce the bifurcation
diagram given by Choi & Joseph (2001). They obtained this diagram by performing
dynamic simulations where the particle was free to move in the transverse direction
as well. Our results are in good agreement with theirs. In fact, we are also able to
plot the unstable branch for the equilibrium height which was not obtained from
the dynamic simulations. From figure 24 we identify the nature of instability of the
equilibrium height; it may be described as a double turning-point bifurcation. The
change of stability at a turning point is not really a bifurcation because a new branch
of solutions does not arise at such a point (see, Iooss & Joseph 1990). The two turning
points give rise to a hysteresis loop depicted in figure 24. Similarly, we can plot the
equilibrium height diagrams for particles of different densities using figure 23.

Implications of multiple steady states for single-particle lifting and on models of
lift-off in slurries should be a subject of future investigation.

## 7. Lift-off of a single particle in plane Poiseuille flows of an Oldroyd-B fluid

In this section we briefly study the effect of fluid elasticity on the lift-off of particles
in plane Poiseuille flows. Figure 25 shows the equilibrium height vs. Deborah number
for a neutrally buoyant particle in an Oldroyd-B fluid. The parameters are as specified
in the figure. A freely rotating neutrally buoyant particle migrates to an equilibrium
radius between the channel centreline and the wall, as in the experiments of Segré &
Silberberg (1961, 1962) with the caveat that the equilibrium radius here depends on
the elasticity parameter. The particle rises more as the fluid elasticity is increased and
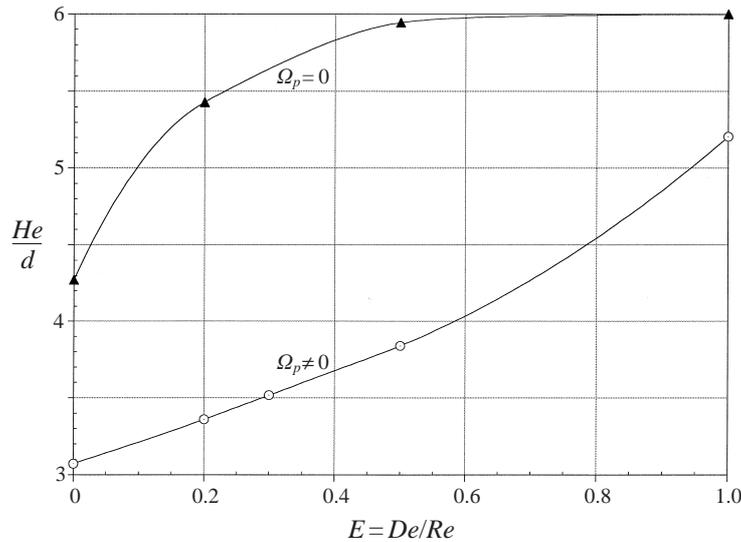non-rotating particles rise even more. In fact, at high enough Deborah numbers, a

FIGURE 25. Lift-off of a circular particle from a horizontal wall in a Poiseuille flow of an Oldroyd-B fluid ($W/d = 12$, $l/d = 22$, $\eta = 1$ poise, $d = 1$ cm, $R = 0.6$).
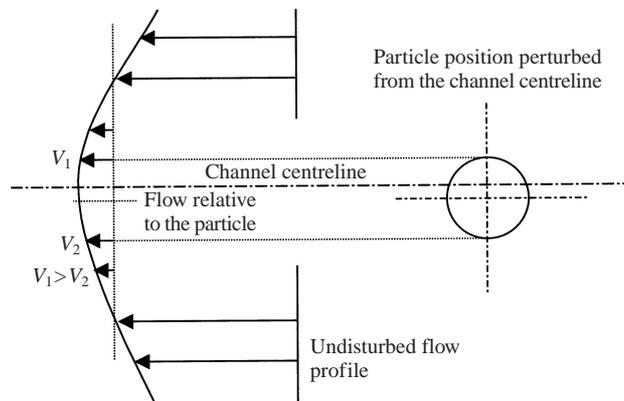


FIGURE 26. Cartoon showing the fluid velocity relative to a non-rotating particle perturbed from the channel centreline in a plane Poiseuille flow.

non-rotating particle migrates all the way to the centre of the channel; the centreline is then a stable position of equilibrium and the Segré–Silberberg effect does not occur.

Figure 26 shows the flow relative to a non-rotating particle in a Newtonian fluid, whose position is displaced from the channel centreline, for typical parameters in our simulations. Relative to the particle the flow comes from the right, both at the top and the bottom of the particle. Similar to the discussion of figure 21, higher incident velocity in the top half ($V_1 > V_2$) of the particle gives rise to higher pressure there. As a result, the particle is pushed further away from the channel centreline, making it an unstable equilibrium position.

Figure 21 shows a particle near the wall of the channel where the hydrodynamic force on the particle is towards the channel centreline, whereas figure 26 shows a particle near the channel centre where the hydrodynamic force is away from the centreline. This is consistent with the Segré–Silberberg effect where the equilibrium
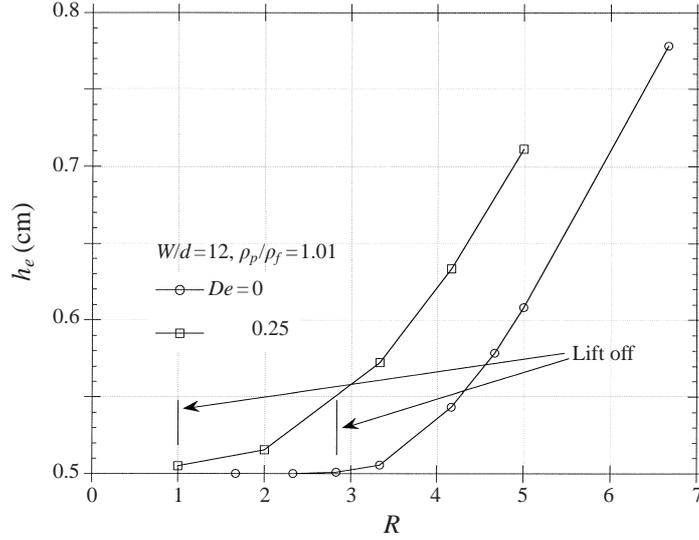
FIGURE 27. Equilibrium height *vs.* shear Reynolds number for a particle in a Poiseuille flow of an Oldroyd-B fluid.

position for a neutrally buoyant particle is between the channel centre and the wall. The velocity of the fluid relative to the particle in its bottom half ($V_2$) changes direction as the particle moves away from the channel centre (figures 21 and 26). This may be associated with the direction of the lift force on the particle.

Figure 27 compares the effect of shear Reynolds number on the equilibrium height of a particle in a Newtonian and an Oldroyd-B fluid. The critical shear Reynolds number for lift-off in an Oldroyd-B fluid is smaller than that in a Newtonian fluid. The particle rises more at higher shear Reynolds numbers. At a given shear Reynolds number the particle rises more in an Oldroyd-B fluid. The fluid elasticity is seen to enhance the lift on a particle. Figure 28 shows the equilibrium height *vs.* Deborah number at a fixed $R$ for a heavy particle. A non-rotating particle rises more. In general, the lift is seen to be greater at higher Deborah numbers.

The stress at any point in an Oldroyd-B fluid can be decomposed as $\boldsymbol{T} = -p\boldsymbol{I} + \eta\boldsymbol{A} + \boldsymbol{\tau}_e$, where $\boldsymbol{\tau}_e$ is the elastic stress. The elastic component of lift $L_e$ on a particle is given by

$$L_e = \oint_{\partial p} \boldsymbol{\tau}_e \cdot \boldsymbol{n} \, \mathrm{d}\Gamma. \tag{23}$$

Only the tangential (or shear) component of $\boldsymbol{\tau}_e \cdot \boldsymbol{n}$ on a rigid surface is non-zero for an Oldroyd-B fluid (Huang, Hu & Joseph 1998; Patankar 1997). The lift fractions are defined as

$$\Phi_p = \frac{L_p}{L_p + L_s + L_e}, \quad \Phi_s = \frac{L_s}{L_p + L_s + L_e}, \quad \Phi_e = \frac{L_e}{L_p + L_s + L_e}, \left.\right\} \tag{24}$$
$$\Phi_p + \Phi_s + \Phi_e = 1.$$

Figure 29 shows the lift fractions *vs.* shear Reynolds number for the cases shown in figure 27. Maximum contribution to the lift force on a particle in an Oldroyd-B fluid comes from the pressure, whereas the elastic stress makes the least contribution. The
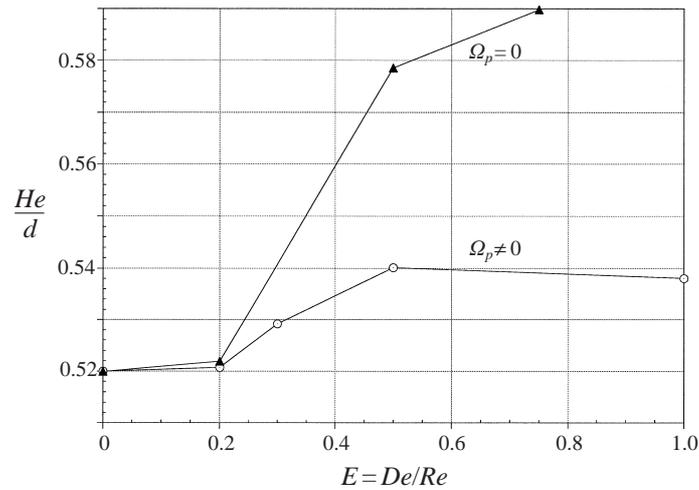
FIGURE 28. Lift-off of a circular particle from a horizontal wall in a Poiseuille flow of an Oldroyd-B fluid ($W/d = 12$, $l/d = 22$, $\eta = 1$ poise, $d = 1$ cm, $\rho_p = 1.001$ g cm$^{-3}$)
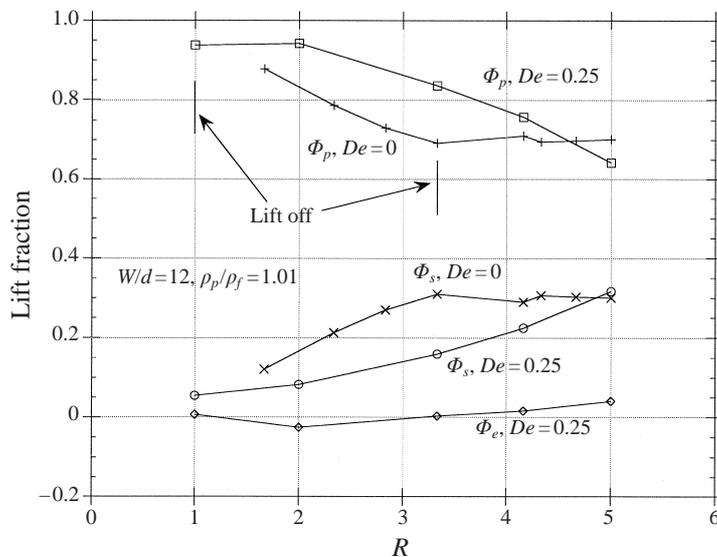


FIGURE 29. Lift fractions *vs.* shear Reynolds number for a particle in a Poiseuille flow of an Oldroyd-B fluid.

pressure lift fraction in an Oldroyd-B fluid is typically larger than that in a Newtonian fluid.

Figures 30($a$)–30($d$) show that a freely moving particle in a Newtonian fluid does not lift off at the given parameters, whereas it lifts off in an Oldroyd-B fluid under similar conditions. The dominant contribution to the lift force comes from the high pressure in the third quadrant (figure 30$d$). The additional upward thrust on the particle in the Oldroyd-B fluid comes from the pressure in the bottom half of the particle, where the shear rate is larger (figure 30$d$) – in agreement with the argument of Joseph & Feng (1996). Figures 30($e$) and 30($f$) show that the contribution to lift
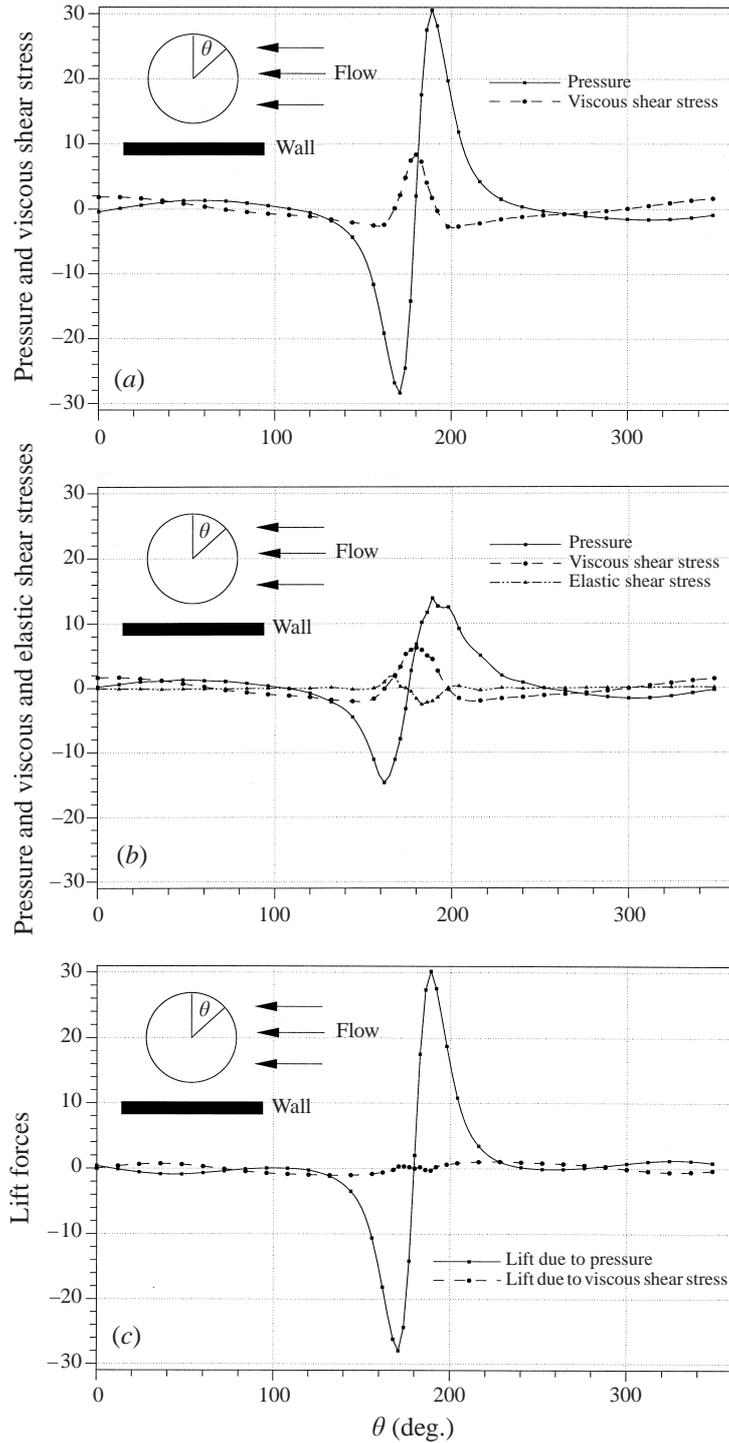
FIGURE 30. (*a*) Distributions of pressure and viscous shear stress on the surface of a freely rotating circular particle in a Poiseuille flow of a Newtonian fluid ($W/d = 12$, $l/d = 22$, $d = 1$ cm, $\rho_p/\rho_f = 1.001$, $R = 0.6$). The particle does not lift-off. (*b*) Distributions of pressure and viscous and elastic shear stresses on the surface of a freely rotating circular particle in a Poiseuille flow of an Oldroyd-B fluid ($W/d = 12$, $l/d = 22$, $d = 1$ cm, $\rho_p/\rho_f = 1.001$, $R = 0.6$, $E = 0.5$). The particle lifts off. (*c*) The distribution of lift forces on the surface of a freely rotating circular particle ($W/d = 12$, $l/d = 22$, $d = 1$ cm, $\rho_p/\rho_f = 1.001$, $R = 0.6$, Newtonian fluid). The particle does not lift off.
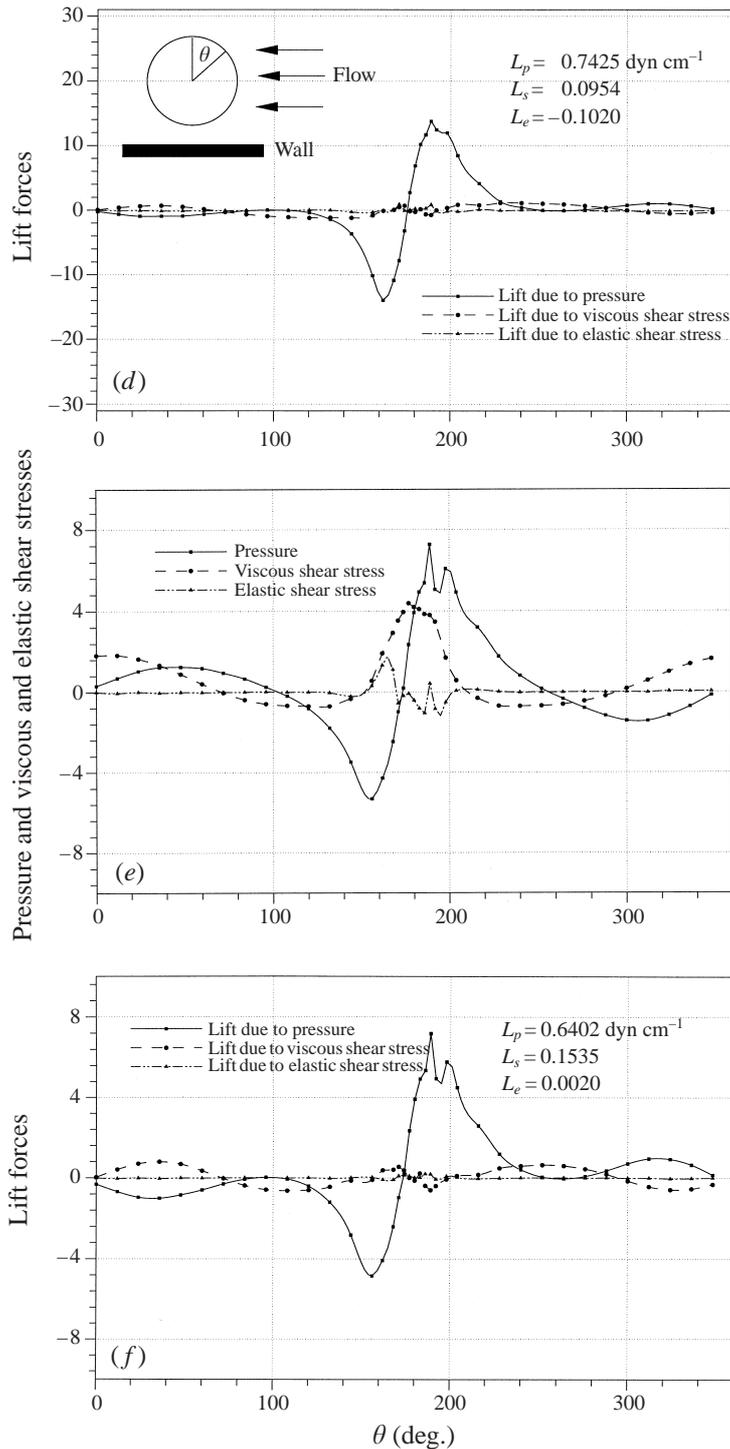
FIGURE 30 (continued). (*d*) The distribution of lift forces on the surface of a freely rotating circular particle ($W/d = 12$, $l/d = 22$, $d = 1$ cm, $\rho_p/\rho_f = 1.001$, $R = 0.6$, $E = 0.5$). The particle lifts off. (*e*) Distributions of pressure and viscous and elastic shear stresses on the surface of a lifted circular particle in a Poiseuille flow of an Oldroyd-B fluid ($W/d = 12$, $l/d = 22$, $d = 1$ cm, $\rho_p/\rho_f = 1.001$, $R = 0.6$, $E = 0.5$, $\boldsymbol{\Omega}_p = 0$). (*f*) The distribution of lift forces on the surface of a lifted circular particle in an Oldroyd-B fluid ($W/d = 12$, $l/d = 22$, $d = 1$ cm, $\rho_p/\rho_f = 1.001$, $R = 0.6$, $E = 0.5$, $\boldsymbol{\Omega}_p = 0$).

from the viscous shear stress is more for a non-rotating particle than for a freely rotating one. The contribution from the pressure is still dominant.

## 8. Summary

We present a brief summary of the results in this paper:

1. We examine the proposition that a freely translating neutrally buoyant sphere (or circle) in an unbounded linear shear flow moves with the fluid and experiences no lift. The result holds for any angular velocity of the particle.

2. If the lift and the buoyant weight of a sphere in an unbounded linear shear flow are in balance then McLaughlin's formula gives rise to at least two values of the slip velocity whereas only one value is obtained by using Saffman's formula (or Bretherton's formula in a two-dimensional case).

3. It is recognized that a moving heavy particle in equilibrium under the balance of weight and lift in an unbounded linear shear flow must be propelled by an external agent to balance the drag.

4. The analytical values of lift and drag from Bretherton's formula are compared with those obtained from numerical simulations. Better agreement is obtained when the slip Reynols number is small.

5. We propose a general data structure for the interrogation of direct numerical simulations that can be used in developing a theory of fluidization by lift.

6. Two-dimensional numerical simulations are performed to study the lift-off of a single circular particle in a plane Poiseuille flow of Newtonian and viscoelastic fluids. After a certain critical shear Reynols number, the particle rises from the wall to an equilibrium height at which the buoyant weight just balances the hydrodynamic lift.

7. A correlation for the critical shear Reynolds number for lift-off is obtained. The critical shear Reynolds number is larger for a heavier particle. Simulations with an Oldroyd-B fluid show that the fluid elasticity reduces the critical shear Reynolds number for lift-off.

8. The equilibrium height of the particle increases with the shear Reynolds number. A larger shear Reynolds number is required to lift a heavier particle to the same height. The dimensionless equilibrium height is larger for a bigger channel at a given shear Reynolds number. The fluid elasticity increases the equilibrium height.

9. Larger values of slip and slip angular velocities are required to balance a heavier particle at the same equilibrium height.

10. The Segré–Silberberg effect (first observed experimentally by Segré & Silberberg 1961, 1962) for a freely moving neutrally buoyant particle in a planar Poiseuille flow is simulated. A smaller rise from the bottom wall is obtained when the slip angular velocity is suppressed. The greater the slip angular velocity, the higher the particle rises. The same effect is observed with an Oldroyd-B fluid. The particle rises more as the fluid elasticity is increased. At high enough Deborah numbers, a non-rotating particle in a Poiseuille flow of an Oldroyd-B fluid moves to the channel centreline at equilibrium, unlike the Segré–Silberberg effect.

11. Simulations of single-particle lift-off at higher shear Reynolds numbers in a Newtonian fluid show multiple steady states and hysteresis loops. This is shown to be due to the presence of two turning points of the equilibrium solution.

12. The contribution to lift from the pressure is seen to be more than that from the viscous shear stress in both Newtonian and Oldroyd-B fluids at low shear Reynolds numbers; they are nearly the same at higher shear Reynolds numbers

in a Newtonian fluid. The elastic shear stress in an Oldroyd-B fluid makes a very small contribution to the lift force and is sometimes negative; the main effect of viscoelasticity is on the pressure.

13. The high pressure on the bottom half of the particle and the viscous shear stress at $\theta = 270°$ are important in determining lift.

## REFERENCES

ASMOLOV, E. S. 1990 Dynamics of a spherical particle in a laminar boundary layer. *Fluid Dyn.* **25**, 886–890.

ASMOLOV, E. S. 1999 The inertial lift on a spherical particle in a plane Poiseuille flow at large channel Reynolds number. *J. Fluid Mech.* **381**, 63–87.

AUTON, T. R. 1987 The lift force on a spherical body in a rotational flow. *J. Fluid Mech.* **183**, 199–218.

BAGNOLD, R. A. 1974 Fluid forces on a body in shear-flow; experimental use of 'stationary flow'. *Proc. R. Soc. Lond.* A **340**, 147–171.

BRENNER, H. 1966 Hydrodynamic resistance of particles at small Reynolds numbers. *Adv. Chem. Engng* **6**, 287–438.

BRETHERTON, F. P. 1962 Slow viscous motion round a cylinder in a simple shear. *J. Fluid Mech.* **12**, 591–613.

CHERUKAT, P. & MCLAUGHLIN, J. B. 1994 The inertial lift on a rigid sphere in a linear shear flow field near a flat wall. *J. Fluid Mech.* **263**, 1–18.

CHERUKAT, P., MCLAUGHLIN, J. B. & DANDY, D. S. 1999 A computational study of the inertial lift on a sphere in a linear shear flow field. *Intl J. Multiphase Flow* **25**, 15–33.

CHOI, H. G. 2000 Splitting method for the combined formulation of fluid–particle problem. *Comput. Meth. Appl. Mech. Engng.* **190**, 1367–1378.

CHOI, H. G. & JOSEPH, D. D. 2001 Fluidization by lift of 300 circular particles in plane Poiseuille flow by direct numerical simulation. *J. Fluid Mech.* **438**, 101–128.

CHORIN, A. J. 1968 Numerical solution of the Navier–Stokes equations. *Math. Comput.* **22**, 745–762.

COX, R. G. & MASON, S. G. 1971 Suspended particles in fluid flow through tubes. *Ann. Rev. Fluid Mech.* **3**, 291–316.

DANDY, D. S. & DWYER, H. A. 1990 A sphere in shear flow at finite Reynolds number: effect of shear on particle lift, drag and heat transfer. *J. Fluid Mech.* **216**, 381–410.

DREW, D. A. & PASSMAN, S. L. 1999 *Theory of Multicomponent Fluids.* Springer.

EICHHORN, R. & SMALL, S. 1964 Experiments on the lift and drag of spheres suspended in a Poiseuille flow. *J. Fluid Mech.* **20**, 513–527.

FEUILLEBOIS, F. 1989 Some theoretical results for the motion of solid spherical particles in a viscous fluid. In *Multiphase Science and Technology* (ed. G. F. Hewitt, J. M. Delhaye & N. Zuber), vol. 4, p. 583. Hemisphere.

FENG, J., HU, H. H. & JOSEPH, D. D. 1994 Direct simulation of initial values problems for the motion of solid bodies in a Newtonian fluid. Part 2. Couette and Poiseuille flows. *J. Fluid Mech.* **277**, 271–301.

FENG, J., HUANG, P. Y. & JOSEPH, D. D. 1995 Dynamic simulation of the motion of capsules in pipelines. *J. Fluid Mech.* **286**, 201–207.

HOGG, A. J. 1994 The inertial migration of non-neutrally buoyant spherical particles in two-dimensional flows. *J. Fluid Mech.* **272**, 285–318.

HU, H. H. 1996 Direct simulation of flows of solid–liquid mixtures. *Intl J. Multiphase Flow* **22**, 335–352.

HU, H. H. & JOSEPH, D. D. 1999 Lift on a sphere near a plane wall in a second-order fluid. *J. Non-Newtonian Fluid Mech.* **88**, 173–184.

HU, H. H. & PATANKAR, N. A. 2001 Simulation of particulate flows in Newtonian and viscoelastic fluids. *Intl J. Multiphase Flow* (to appear).

HU, H. H., PATANKAR, N. A. & ZHU, M.-Y. 2001 Direct numerical simulations of fluid–solid systems using the arbitrary Lagrangian–Eulerian technique. *J. Comput. Phys.* (to appear).

HUANG, P. Y., FENG, J., HU, H. H. & JOSEPH, D. D. 1997 Direct simulation of the motion of solid particles in Couette and Poiseuille flows of viscoelastic fluids. *J. Fluid Mech.* **343**, 73–94.

HUANG, P. Y., HU, H. H. & JOSEPH, D. D. 1998 Direct simulation of the sedimentation of elliptic particles in Oldroyd-B fluids. *J. Fluid Mech.* **362**, 297–325.

IOOSS, G. & JOSEPH, D. D. 1990 *Elementary Stability and Bifurcation Theory.* 2nd edn. Springer.

JOSEPH, D. D. 2001 Interrogations of direct numerical simulation of solid–liquid flow. http://www.aem.umn.edu/Solid-Liquid_Flows/.

JOSEPH, D. D. & FENG, J. 1996 A note on the forces that move particles in a second-order fluid. *J. Non-Newtonian Fluid Mech.* **64**, 299–302.

JOSEPH, D. D., LIU, Y. J., POLETTO, M. & FENG, J. 1994 Aggregation and dispersion of spheres falling in viscoelastic liquids. *J. Non-Newtonian Fluid Mech.* **54**, 45–86.

KRISHNAN, G. P. & LEIGHTON, D. T. 1995 Inertial lift on a moving sphere in contact with a plane wall in a shear flow. *Phys. Fluids* **7**, 2538–2545.

KUROSE, R. & KOMORI, S. 1999 Drag and lift forces on a rotating sphere in a linear shear flow. *J. Fluid Mech.* **384**, 183–206.

KUETHE, A. & CHOW, C. Y. 1998 *Foundations of Aerodynamics*, 5th edn. John Wiley.

LEAL, L. G. 1980 Particles motions in a viscous fluid. *Ann. Rev. Fluid Mech.* **12**, 435–476.

LEIGHTON, D. T. & ACRIVOS, A. 1985 The lift on a small sphere touching a plane in the presence of a simple shear flow. *Z. angew. Math. Phys.* **36**, 174–178.

LIN, C., PEERY, J. H. & SCHOWALTER, W. R. 1970 Simple shear flow round a rigid sphere: inertial effects and suspension rheology. *J. Fluid Mech.* **44**, 1–17.

LIU, Y. J. & JOSEPH, D. D. 1993 Sedimentation of particles in polymer solutions. *J. Fluid Mech.* **255**, 565–595.

LIU, Y. J., NELSON, J., FENG, J. & JOSEPH, D. D. 1993 Anomalous rolling of spheres down an inclined plane. *J. Non-Newtonian Fluid Mech.* **50**, 305–329.

LIU, Y. J., POLETTO, M., FENG, J. & JOSEPH, D. D. 1994 Agregation and dispersion of spheres falling in viscoelastic liquids. *J. Non-Newtonian Fluid Mech.* **54**, 45–86.

MCLAUGHLIN, J. B. 1991 Inertial migration of a small sphere in linear shear flows. *J. Fluid Mech.* **224**, 261–274.

MEI, R. 1992 An approximate expression for the shear lift force on a spherical particle at finite Reynolds number. *Intl J. Multiphase Flow* **18**, 145–147.

PATANKAR, N. A. 1997 Numerical simulation of particulate two-phase flow. PhD thesis, University of Pennsylvania.

RICHARDSON, J. F. & ZAKI, W. N. 1954 Sedimentation and fluidization: Part I. *Trans. Instn Chem. Engrs* **32**, 35–53.

RUBINOW, S. I. & KELLER, J. B. 1961 The transverse force on a spinning sphere moving in a viscous fluid. *J. Fluid Mech.* **11**, 447–459.

SAFFMAN, P. G. 1965 The lift on a small sphere in a slow shear flow. *J. Fluid Mech.* **22**, 385–400; and Corrigendum 1968 *J. Fluid Mech.* **31**, 624.

SEGRÉ, G. & SILBERBERG, A. 1961 Radial Poiseuille flow of suspensions. *Nature* **189**, 209.

SEGRÉ, G. & SILBERBERG, A. 1962 Behaviour of macroscopic rigid spheres in Poiseuille flow. Part 2. Experimental results and interpretation. *J. Fluid Mech.* **14**, 136–157.

SINGH, P. & JOSEPH, D. D. 2000 Sedimentation of a sphere near a vertical wall in an Oldroyd-B fluid. *J. Non-Newtonian Fluid Mech.* **94**, 179–203.

YE, J. & ROCO, M. C. 1992 Particle rotation in a Couette flow. *Phys. Fluids* A **4**, 220–224.

ZHU, M.-Y. 2000 Direct numerical simulation of the solid–liquid flows of Newtonian and viscoelastic fluids. PhD thesis, University of Pennsylvania.